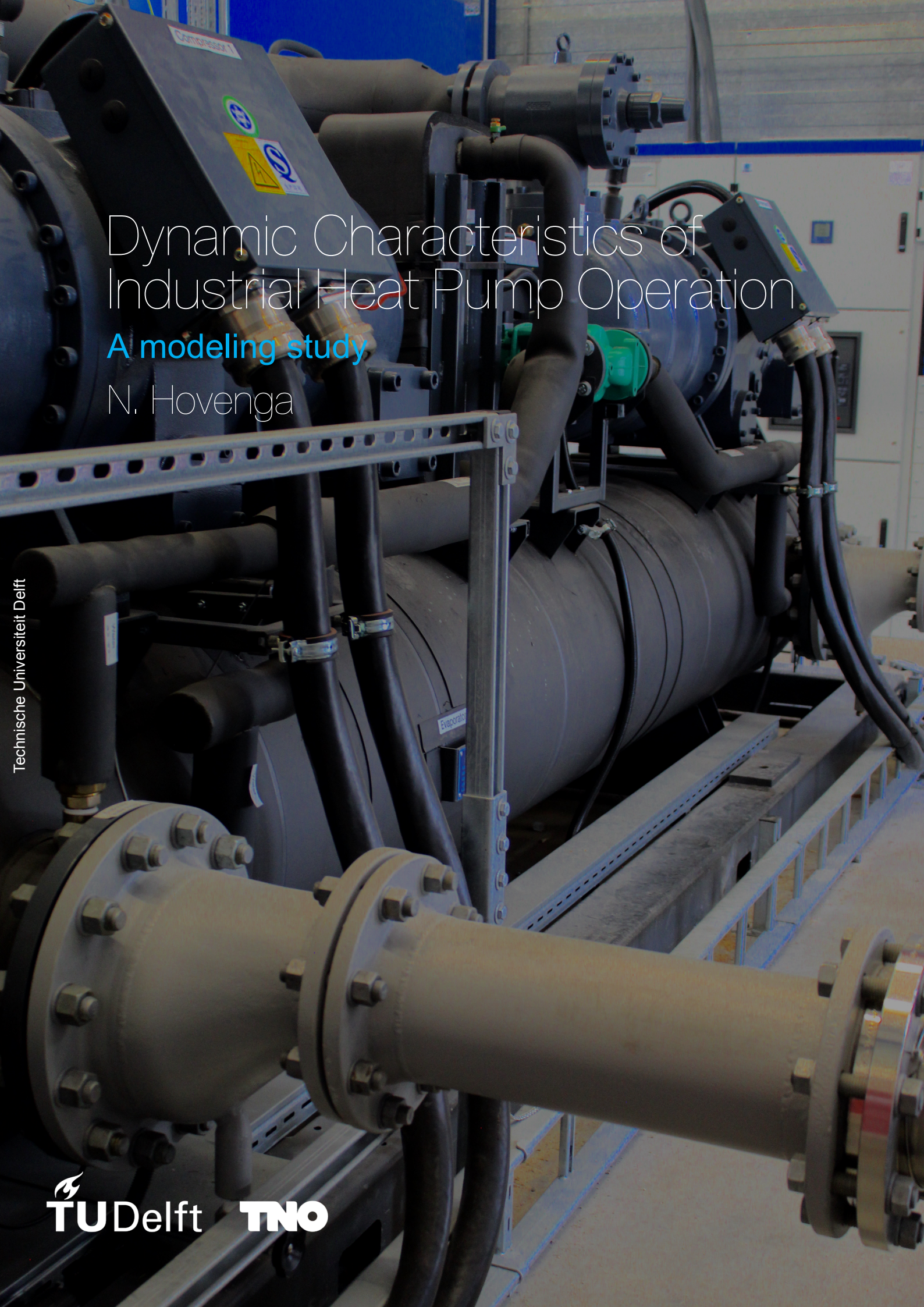

Dynamic Characteristics of Industrial Heat Pump Operation

A modeling study

N. Hovenga

Technische Universiteit Delft

TU Delft TNO

Dynamic Characteristics of Industrial Heat Pump Operation

A modeling study

by

N. Hovenga

to obtain the degree of Master of Science
at the Delft University of Technology,
to be defended publicly on Friday July 9, 2021 at 14:00.

Student number:	4367154	
Project duration:	November 16, 2020 – July 9, 2021	
Thesis committee:	Prof. dr. ir. B.J. Boersma,	TU Delft, supervisor
	Prof. dr. ir. S. Klein,	TU Delft
	Dr. ir. R. Pecnik,	TU Delft
	Dr. ir. M.J.B.M. Pourquie,	TU Delft
	Dr. ir. G.J. Otero Rodriguez	TNO

An electronic version of this thesis is available at `http://repository.tudelft.nl/`.

TU Delft

Abstract

In order to reach the goals of the Paris Agreement, global emissions must decrease at a steady rate of 7.6% each year to 2050 [38]. This rate equals the impact of more than one COVID-19 pandemic per year, for the next 30 years [22]. Looking at the industrial sector, the largest share of energy is used for process heating, with fossil fuels as its primary source [20]. A key technology to improve the energy efficiency and reduce the emissions of process heating is by the integration of heat pump technology.

However, operational costs are still a limiting factor in the widespread uptake of this technology. A potential of industrial heat pumps that will have a positive effect on the operational costs, as well as its general applicability, is the possibility to operate the equipment in a flexible manner. At this point, the potential to respond with high temperature industrial heat pumps to heat demand, the electricity market or to grid congestion, is not yet unlocked.

The focus in this study is on gaining more insight into the dynamic characteristics of high temperature industrial heat pump operation. The approach to do so is based on modeling of a high temperature industrial heat pump in the Dymola simulation environment. With this model, the control strategy can be optimized and the dynamic limitations can be identified. The approach is conservative in its nature, to allow for modeling errors as experimental validation is out of the scope.

The modeling environment is block diagram based, which allows for independent development of the individual heat pump components. Because the screw compressor in the heat pump cycle has an intermediate injection port, a customized model is used to describe the behavior. Despite some adjustments, this model is in its basis based on the model described by Dardenne et al. [19]. The compressor model is calibrated using performance data supplied by the manufacturer.

The heat exchanger models are based on the commercial TIL-suite library [66] and are discretized using the finite volume method. A grid independence study is used to determine the required grid refinement. The fully assembled heat pump model performance is validated using a steady state analysis. In contrast to the steady state analysis, the refrigerant charge is of importance in the dynamic model and needs to be adapted to match the heat pump performance.

By running multiple simulations, the dynamics of the heat pump are identified over a range of operating conditions. Based on the derived coupling between subsystems, a suitable control strategy is selected. The system dynamics are used to tune the controllers with the tuning algorithm by Mathworks. After validation of the controller performance and robustness, the PID SISO control structure is concluded to be a suitable solution. A benefit of this solution is the accessibility for industry and the absence of more complex tuning studies. The implementation of additional control structures is also looked into, and disturbance rejection based feedforward can lead to even higher performance.

Quantitatively speaking, the industrial high temperature heat pump considered in this report is found to be able to ramp up and down at a maximum rate of 20%/min. The limiting factor in this economizer based cycle is the ability of the control system to keep the superheat at the screw compressor injection port within acceptable limits. This level of flexibility allows use of the heat pump for both demand and electricity price response, as well as for participation in grid load balancing pools. On a higher level, based on these results flexible heat pump operation can be considered possible.

A dynamic limitation identified is related to the maximum increase rate of the evaporator water temperature. This is considered relevant for all heat pump systems, and concerns condensation in the compressor suction line. Because the developed model cannot be used for quantification of this problem, this should be addressed in future studies. The same goes for the experimental validation of the heat pump model. This is considered a valuable next step in demonstrating the flexibility.

Preface

This thesis concludes my Master study in Mechanical Engineering at the Delft University of Technology. I have worked on this thesis project at TNO, within the department 'Sustainable Technology for Industrial Processes'.

I want to thank Andrew Marina and Robert de Boer for the opportunity to work on this challenging project, and for their valuable help along the way. I also want to thank Gustavo Otero Rodriguez and Wouter de Vries for their advice, especially during the final months of the project.

I am also grateful to Bendiks Jan Boersma, my academic supervisor. The discussions we had have been very helpful. This was not limited to technical aspects, but helped me to adapt the project scope to changing circumstances already at an early stage.

Lastly I want to thank my family and friends, who have supported me not only during the thesis project, but during the Master study in general. Without your help, this would not have been possible.

N. Hovenga
Delft, July 2021

Contents

List of Figures

List of Tables

Nomenclature

Latin Symbols

A	Area	m^2
C	Flow coefficient	-
E	Energy	J
e	Error	-
f	Friction factor	-
g	Gravitational constant	$\mathrm{m/s}^2$
G	Gain	-
h	Specific enthalpy	$\mathrm{J/kg}$
h_b	Pool boiling heat transfer coefficient	$\mathrm{J/(m^2 \cdot K \cdot s)}$
h_d	Discharge chamber heat transfer coefficient	$\mathrm{J/(m^2 \cdot K \cdot s)}$
h_0	Reference enthalpy	$\mathrm{J/kg}$
H	Enthalpy	J
k	Thermal conductivity	$\mathrm{J/(m \cdot K \cdot s)}$
Kd	Derivative gain	-
Ki	Integral gain	-
Kp	Proportional gain	-
Kv	Flow coefficient	$\mathrm{m^3/h}$
m	Mass	kg
$\dot{m}$	Mass flow rate	$\mathrm{kg/s}$
n	Frequency	Hz
Nu	Nusselt number	-
p	Pressure	Pa
P	Power	$\mathrm{J/s}$
Pr	Prandtl number	-
Q	Heat transfer rate	$\mathrm{J/s}$
q	Heat flux	$\mathrm{J/(m^2 \cdot s)}$
Ra	Rayleigh number	-
Re	Reynolds number	-
T	Temperature	K
t	Time	s
Td	Derivative time	-
Ti	Integration time	-
U	Internal energy	J
u	Input signal	-
V	Volume	m^3
v	Velocity	$\mathrm{m/s}$
Vi	Internal volume ratio	-
W	Work	J
Y	Expansion factor	-
y	Output signal	-
Z	Compressibility factor	-
z	Height	m

Greek Symbols

β	Thermal expansion coefficient	$1/\mathrm{K}$
γ	Heat capacity ratio (c_p/c_v)	-
η	Efficiency	-

Λ	Relative gain array	-
ν	Kinematic viscosity	m^2/s
ρ	Density	kg/m^3

Subscripts

a	Upstream
amb	Ambient
b	Downstream
comp	Compressor
cv	Control volume
dis	Discharge
elec	Electric
ff	Feedforward
hs	High stage
ht	Heat transfer
inj	Injection
leak	Leakage
ls	Low stage
mot	Motor
ms	Mid stage
sat	Saturated
suc	Suction
w	Wall

Abbreviations

CAPEX	Capital Expenditures
COP	Coefficient of Performance
DASSL	Differential Algebraic System SoLver
EES	Engineering Equation Solver
FOPDT	First Order Plus Dead Time
MIMO	Multi Input, Multi Output
RGA	Relative Gain Array
SISO	Single Input, Single Output
SOPDT	Second Order Plus Deadtime Model
TRL	Technical Readiness Level
VFD	Variable Frequency Drive

1 Introduction

1.1. Background

Global greenhouse gas emissions in 2020 are drastically reduced due to the COVID-19 pandemic. The average annual greenhouse gas emissions in 2020 are expected to be 7% less than in 2019 [38]. Despite this being welcome news in the battle against climate change, it also provides a worrying perspective to the Paris Agreement. The Emission Gap Report, which is recently published [71], shows that in order to reach the goals of the Paris Agreement, global emissions must decrease at a steady rate of 7.6% each year to 2050. In other words, more than the impact of one COVID-19 pandemic is needed each year for the next 30 years, to reach the Paris Agreement goals [22].

This analogy stresses the importance of continuing and intensifying the battle against greenhouse gas emissions. The total energy demand of the European industry in 2019 is depicted in figure 1.1. Note that the majority of the energy, 66%, is used for process heating purposes. No less than 78% of the process heating energy demand is covered by fossil fuels [20]. As stated by the International Energy Agency, greater ambition is needed to increase the share of renewables for heat and to improve energy efficiency [29].

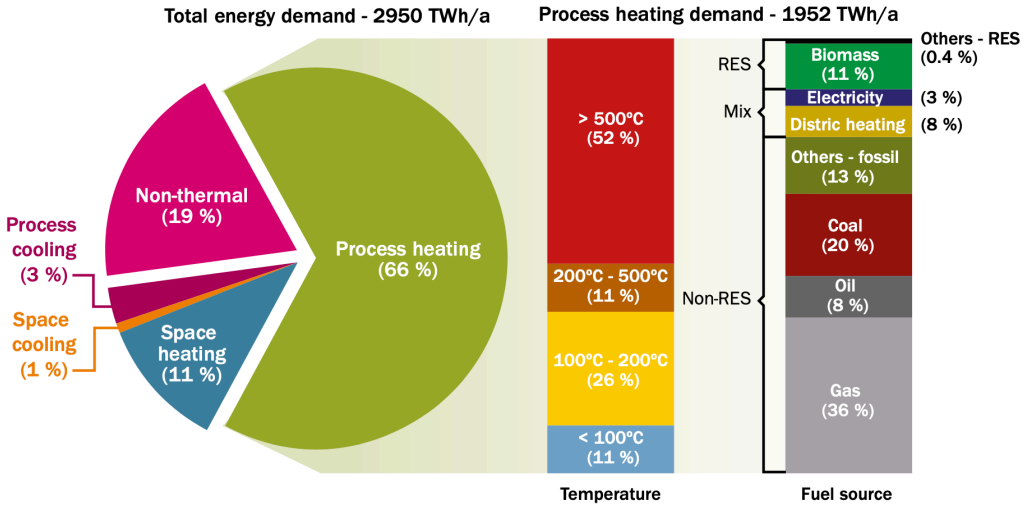

Figure 1.1: Industrial energy consumption in Europe in 2019 [20]

In the light of this ambition, a key technology to improve energy efficiency is by the integration of heat pump technology. This technology has a large potential in lowering the loss of thermal energy in industrial processes [20]. Note that the applicability of heat pumps does however highly depend on the desired temperature levels, also included in figure 1.1. Industrial processes with a temperature range

up to 100°C can already be supplied with today's heat pump technology [11]. The so-called high temperature industrial heat pump technology, with sink temperatures in the range of 100 - 200°C, is still in the development phase. Although pioneering companies have already started commercialising industrial heat pumps with sink temperatures up to 165°C [34], further research is needed to accelerate widespread integration. Industrial high temperature heat pumps are of particular interest for steam production. Steam is the preferred heat carrier in many industrial production processes [70]. Typical industries where steam within the aforementioned temperature range is used is the food, paper and chemicals industry [11].

One particular barrier limiting widespread integration is the investment case still not being sufficiently attractive [20]. This barrier can be split into two different aspects. The first aspect is that the capital expenditure (CAPEX) is still too high. Both the equipment and the integration study are costly. These costs are correlated with the Technical Readiness Level (TRL), and will go down when the equipment becomes more mass produced [53]. At this moment in time, customization for every process is still the norm.

The second aspect that affects the investment case is the operational expenditure. With increasing cycle efficiency, the investment case will become more interesting. Various research initiatives aim at improving the cycle efficiency. This for example by applying new refrigerants or advanced cycles [49][10]. A potential which is not yet unlocked, is the ability to operate industrial heat pumps in a flexible manner. Various studies have shown the positive effect of this feature on operational costs [68]. Flexible operation, also called smart operation, allow the hardware to react to the process demand, the electricity price and to grid congestion.

1.2. Research questions

The focus in this study is on the ability of high temperature industrial heat pumps to operate in a flexible manner. In order to gain insight to what extent industrial heat pumps can be used for process demand and electricity price response, a subdivision is made into the following questions. Answers to these research questions are constructed throughout this report.

1. What is a suitable method to model the individual heat pump components?
2. What is the most suitable control method for flexible heat pump operation?
3. What are the dynamic characteristics of industrial heat pump operation?

1.3. Methodology

Because of practical limitations, as well as the high costs that go together with equipment on the industrial scale, studying the dynamics either by changing the actual design or by trial and error, is not considered feasible. Therefore, a dynamic model is developed that simulates the dynamics of an industrial heat pump. This also allows for a more thorough investigation of the internal phenomena that happen during dynamic operation.

A step-wise method is applied in developing the dynamic model. First of all, the individual heat pump components are modeled separately, using the Modelica object-oriented language [48] and the commercial library TIL Suite [66]. Performance data supplied by the manufacturer is used to calibrate the component models. Extra attention is paid to the development of the compressor model, because of the relatively complex behaviour.

Next, the individual heat pump component models are assembled. The steady state performance of the complete heat pump model is validated using a performance analysis based on data supplied by the heat pump manufacturer.

The most suitable control method is determined by performing a coupling and time delay analysis between in- and outputs. The settings of the selected control method are tuned based on a linearized system identification at multiple operating conditions. Next, the control method is implemented and the robustness is analysed. Finally, the dynamic characteristics of the heat pump are investigated using the model, and the limitations are identified.

1.4. Scope

The developed dynamic model can be used for the simulation of industrial heat pumps. In this study the model is applied to the 2 MW closed economizer heat pump developed by Ochsner, as described in more detail in subsection 2.1.3.

1.5. Outline

An analysis of the problem is presented in chapter two. This chapter covers details of industrial heat pumps, such as the cycle design and the current state of technology. Also the compressor technology is analyzed. An analysis of previous work related to heat pump dynamics is presented, followed by an overview of the experimental facility on which the model is based.

In chapter three, a brief discussion is presented on the different modeling environments available. Next, the model development of the individual heat pump components is presented; the compressor, the heat exchangers, the expansion valves and the piping. The chapter is concluded by discussing the simulation setup. The calibration and validation of the individual heat pump component models is presented in chapter four. Also the steady state validation of the assembled heat pump model is presented.

In chapter five the focus is on the optimization of the heat pump controls for flexibility. First an analysis is presented from which the most suitable control method follows. Next, the tuning of controllers along with a robustness test is presented. The second part of this chapter covers the actual investigation into the dynamic characteristics of the industrial heat pump, for both load level changes as well as for changes in evaporator water temperature.

2

Problem analysis

In order to gain more insight into the dynamic characteristics of industrial heat pump operation, first an analysis into the problem is required. In this chapter, the problem is analyzed by focusing on the industrial heat pump market and the state of technology first. Next, the focus shifts to the component level, where the compressor technology and modeling are discussed. In the third section, an overview of previous heat pump modeling work is presented. In the final section, the research facility is discussed that will be used to follow up on the work presented in this study.

2.1. Industrial heat pumps

2.1.1. Market potential

In recent years, various studies investigating the high temperature industrial heat pump market potential are published. The majority of these studies focused on identifying the high temperature heat demand in industry, while neglecting the available waste heat supplies [54]. A study that did include the available waste heat supply was published by Kosmadakis in 2019 [36]. In this study, the focus is on heat pumps with sink temperatures in the range of 100 - 200°C. The value of this work is limited because of the fact that the technical readiness level is not equal throughout the temperature range. A study that does include this aspect as well is published recently by Marina et al. [43] This study applies a bottom-up approach and is aimed at providing heat pump manufacturers with a market perspective. Both the heat demand and the available waste heat are included in this market potential investigation, in which characteristics such as the temperature level and performance are included as well. Note that this study focused on the the European Union.

In general, a similar conclusion is found in the different high temperature heat pump market potential studies; namely that a large market potential is identified. As mentioned in the study by Marina et al. [43], the investment needed to cover the market potential is estimated in the range of €4.60 - €11.5 billion. This market potential only covers the paper, chemical, food and refinery industry, in which the chemical and paper sector have the biggest share. Because of the bottom-up approach, this is a conservative estimate.

2.1.2. Current state of technology

As mentioned by both Apargaus [11] and Marina et al. [43], industrial high temperature heat pumps in the range of 100°C to approximately 150°C are made commercially available by a few pioneering companies, although further research is needed to strengthen the understanding of the technology. Both studies also mention that in the higher temperature range of 150 - 200°C, further research is needed in order to make the technique ready for adoption by heat pump manufacturers.

A wide variety of cycle designs is applied. As presented in the study by Arpagaus [8], Kobe Steel is promoting their Kobelco SGH 165 high temperature industrial heat pump as the first of its kind able to produce steam at a temperature of 165°C. Do note that for this, a source of steam already at 120°C is needed. The high temperature heat pump HeatBoosterR245fa, commercialised by Viking, has a

maximum heat sink temperature of 150°C. The cycle of this heat pump is based on a single stage design with an internal heat exchanger (IHX) and a storage vessel. More details related to the cycle design are covered in subsection 2.1.3.

The Austrian company Ochsner has build two different high temperature industrial heat pumps with sink temperatures up to 130°C. The IWWDSS R2R3b is a two stage heat pump. The low pressure stage uses R134a as refrigerant, and in the high pressure stage the by Ochsner developed refrigerant Öko1, which is based on R245fa, is used. The IWWDS ER3b is a one stage heat pump and uses Öko1 as refrigerant. Both heat pumps use single screw compressors, and the maximum heating capacity is 1.5 MW. A newly developed heat pump is build by Ochsner for research purposes specifically and is installed at TNO in Petten. This heat pump has a heating capacity of 2 MW at a nominal conditions. This heat pump is discussed in more detail in subsection 2.4.1.

The lower the sink temperature, the higher the TRL, and consequently the more heat pumps have become available. At a sink temperature of 120°C, Hybrid Energy offers the highest capacity heat pump, with a heating capacity of up to 2.5 MW. Combitherm, Mayekawa and Kobelco also offer heat pumps with a sink temperature up to 120°C, but with significantly lower heating capacities, below 400 kW [11].

The current state of technology is pushed forward by various research initiatives [11]. Most initiatives are supported by experimental studies. Noteworthy is that the majority of the experimental studies is focused on heat pumps with heating capacities in the order of tens of kilowatts (lab-scale), or hundreds of kilowatts (prototype-scale). The main research goals are increasing the heat pump efficiency by testing new cycle designs and compression technologies, testing new environmentally friendly refrigerants and achieving higher sink temperatures.

The refrigerant selection is also highly subject to innovation pushed by the climate crisis. Refrigerants that were common in refrigeration systems are found to have very high Global Warming Potentials (GWP). The GWP is a measure of how much heat the gas traps in the atmosphere. To illustrate the effect of refrigerants; the common R134a has a GWP of 1430, meaning the effect of this medium is 1430 times stronger than CO2 on the greenhouse gas effect. [69] Another aspect relevant to refrigerants is the Ozone Depletion Potential. As the name suggests, this number quantifies the refrigerant's potential to deplete the ozone layer.

Apart from these two characteristics, the influence of the refrigerant type on the high temperature heat pump cycle efficiency and the heat pump component design is also important. At high temperature lifts, a high coefficient of performance (COP) is desired as well. This can be challenging, due to the decreasing enthalpy of vaporization at higher pressures. Also the volumetric heat capacity is of importance, as this influences the heat pump component sizing. Innovative refrigerants that score well in terms of efficiency, environmental potentials, flammability and toxicity, are R1233zd(E) and R1224yd [11] [7] [27].

2.1.3. Advanced cycles

As became clear in the previous section, various advanced cycle layouts are implemented by the high temperature heat pump manufacturers. The goal of these advanced cycles is increasing the performance of the cycle, either by increasing the temperature lift or by increasing the efficiency. Another reason for complicating the design is for safety. It must be noted that a compromise needs to be made, because complicating the cycle design goes hand in hand with an increase in CAPEX. In this section, the cycle design of the Kobe Steel Kobelco SGH 165 and Viking HeatBooster S4 heat pump will be touched upon. Also the cycle design of the newly developed Ochsner heat pump is discussed.

The Kobe Steel Kobelco SGH 120/165 is a standard vapor compression heat pump on the bottom cycle, combined with an open steam compression unit as the top cycle. In the latter, the steam temperature is raised to 165°C. See figure 2.1. The Viking HeatBooster S4 employs a slightly more advanced cycle, as visualised in figure 2.2. Both figures are based on Arpagaus [11]. In this cycle, a piston compressor, a flash tank and an IHX are integrated. The IHX is used to provide superheat after the evaporator.

For some refrigerants, part of the saturated vapor boundary slope in the pressure-enthalpy diagram is lower than the slope of the constant entropy lines [39], see figure 2.4. The superheat is required to ensure that during the compression step sufficient margin to the two-phase region is available. Liquid formation in the compressor is undesired and could potentially damage the compressor [49]. From the study by Moisi et al. [49], it becomes clear that the use of the IHX has a positive effect on both the heating capacity and the COP.

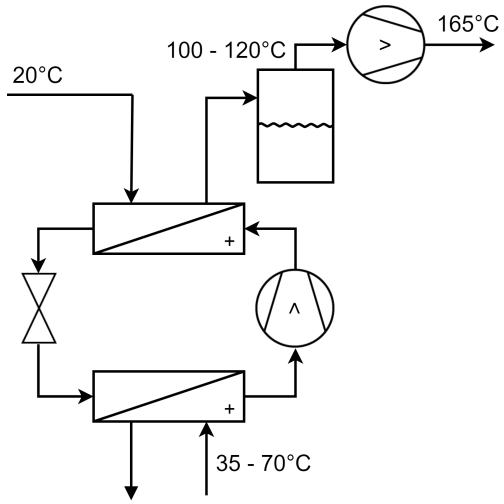

Figure 2.1: Kobe Steel Kobelco SGH 165 cycle layout

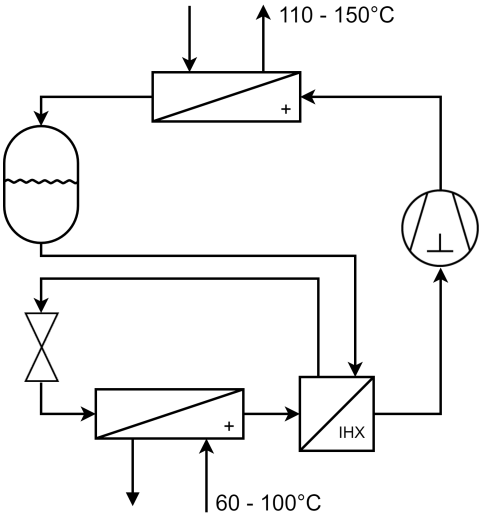

Figure 2.2: Viking HeatBooster S4 cycle layout

The recently developed Ochsner heat pump is based upon the closed economizer cycle, as presented in figure 2.3. The pressure enthalpy-diagram is presented in figure 2.4. In this cycle, the condensed fluid is split into two; the main condensate that flows to the evaporator, and a smaller fraction that will flow to the injection port of the screw compressor. The main condensate stream is first subcooled by the injection stream, and consequently expanded before it flows to the evaporator. The flow through the injection line is first expanded, and then used to subcool the main condensate stream. The heat is exchanged in the economizer. This cycle is also studied by Moisi et al. [49], and is found to have a higher efficiency than the cycle applied by Kobe Steel. Note that in this cycle the required superheat needs to be provided by the evaporator. Both Arpagaus [11] and Moisi et al. [49] present the economizer cycle to be too complicated in comparison to the basic IHX cycle, and therefore not competitive. This is however not well substantiated, as cost specific analysis is missing.

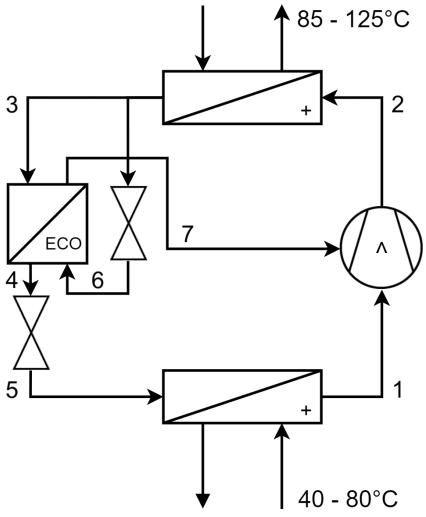

Figure 2.3: Ochsner economizer cycle layout

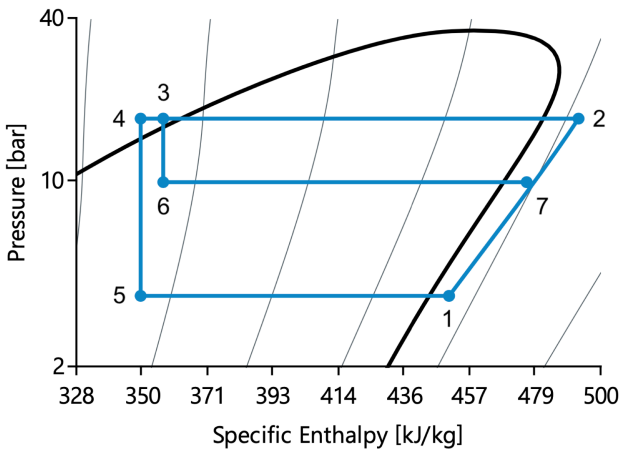

Figure 2.4: Pressure-enthalpy diagram of the economizer cycle with constant entropy lines

2.2. Screw compressors

2.2.1. Technology

Screw and piston compressors are commonly used in high temperature industrial heat pumps. Screw compressors are the preferred choice for high capacity heat pumps (0.08 - 6.00 MW) [28]. This is because of the smaller footprint, the more continuous flow rate and the smaller number of moving parts. The smaller number of moving parts is advantageous from a maintenance point of view. For the same reason, twin screw compressors are more common than single screw compressors.

Twin screw compressors consist of a male and a female helical shaft, oriented parallel to each other. See figure 2.5. The shafts are enclosed in the housing, in which the inlet and outlet are situated on opposite sides. A cavity between the two screws is present, which is reduced over the length of the screws. The ratio at which this volume is reduced is a geometrical property of the compressor and is called the internal volume ratio Vi.

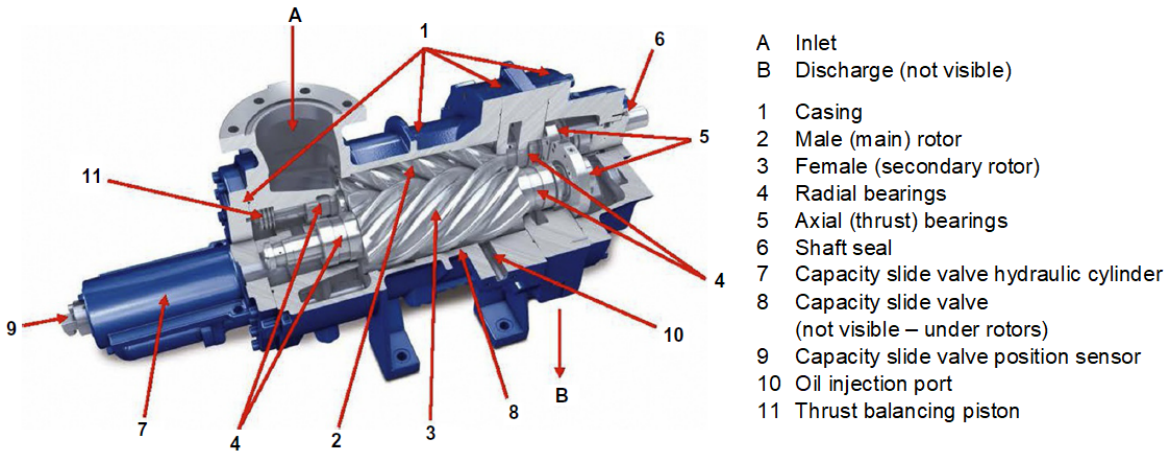

Figure 2.5: Oil flooded twin-screw compressor main components [14]

In heat pump applications, it is common to have oil injection into the compression chamber for two reasons; to seal the built-in clearances between the screws and the housing, and to lubricate the contact area between the screws. In oil injected twin-screw compressors, only one of the screws is driven by the electric motor, and the other screw is fully driven by the contact area. The oil sealing in the clearances limits refrigerant back-flow. A limited amount of oil, in which refrigerant is dissolved, will flow upstream because of the pressure difference [73].

Due to the built in volume ratio Vi, the design of the screw compressor should be matched accurately with the operating conditions. If the design and the operating conditions are not well matched, either under or over-compression occurs [28]. This negatively affects the efficiency. In the case of under-compression, back-flow in the discharge port will occur. The effects of under- and over-compression are visualised in figure 2.6, in which the marked area quantifies the additional losses.

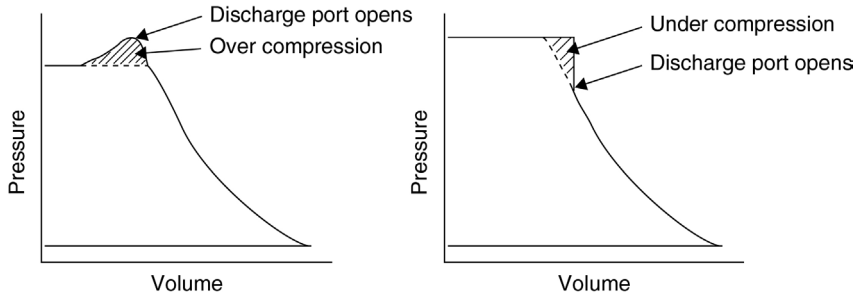

Figure 2.6: Indicator diagram for compressors with built-in volume ratio, to illustrate over- and undercompression effects [28]

The capacity of the screw compressor can be controlled in two different ways. First of all, a variable frequency drive (VFD) can be installed on the electric motor. By varying the frequency and thus the compressor speed, the capacity is adjusted. The second method is by adjusting the so-called slide valve position. The slide valve is situated centralised below the two screws. A schematic representation is given in figure 2.7. If the valve slides to the right, a gap occurs through which the the gas can flow back to the suction line. The further the valve is moved, the larger the gap, and the more the capacity is reduced. In current screw compressors, the capacity can be reduced by up to 90% using the slide valve. Slide valve control is often restricted to four fixed positions, but can be stepless as well. A comparison between a VFD and a slide valve controlled twin-screw compressor is described by the International Refrigeration Consortium in 2004 [32] and by Shah et al. in 2015 [63]. From the presented studies capacity control by VFD is found to be more energy efficient compared to slide valve control below 95% part load. At full load conditions, approximately 3% more energy is consumed in a VFD controlled compressor due to higher electrical power losses. Taking into account the lower installed costs of the slide valve in comparison with the VFD, the most suitable control method will be application dependent.

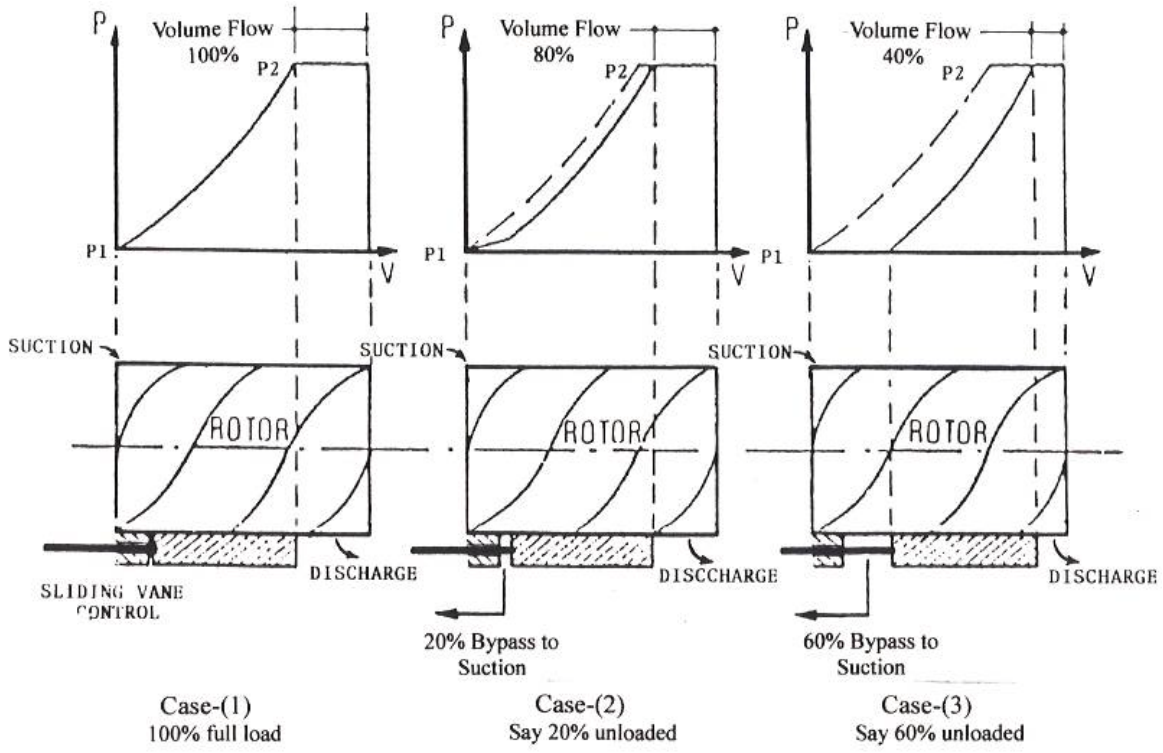

Figure 2.7: Slide valve capacity control [76]

Screw compressors are an excellent choice for application in economizer heat pump cycles. This because in contrast to piston compressors, refrigerant can be injected continuously into the screw cavity at an intermediate pressure. Note that the same is possible with scroll compressors, because of the practically identical working principle of of both types. With some refrigerants, an added advantage of injection is that the already partly compressed refrigerant from the suction line can be cooled slightly. The screw compressor could therefore start to behave more like a two-stage intercooled compressor, with reduced required compressor work and reduced outlet temperature. This last advantage, the reduced outlet temperature, is of importance as the compression end temperature is subject to technical limitations. The compression end temperature should not exceed ±150°C. With today's technology, this is the maximum temperature at which lubricity and oil tightness can be ensured [11].

2.2.2. Modeling

Due to the benefits of refrigerant injection, various studies have focused on developing mathematical models to support performance analysis. Because of the previously mentioned similarity between both compressor types, models for screw and scroll compressors are interchangeable, and are therefore both considered. A subdivision can be made between empirical, semi-empirical and geometrical models. The empirical models require a full dataset to describe the compressor performance, and are especially suitable to implement in complex thermodynamic systems in which no analysis on the component level is required. If the goal of the model is use in the detailed design phase, they are not suitable. For this, geometrical models are developed. Semi-empirical models are in between, and use both geometrical and empirical data. A clear overview of the published scroll compressor models is presented by Byrne in 2014 [15], from which it becomes clear that most models are geometrical. However, even for geometrical models experimental calibration might still be necessary. In the thesis of Van Bommel [73], a full geometrical model is presented, where experimental calibration is still needed.

For the twin-screw compressor that will be modeled in this study, no detailed geometrical specifications are available. Because insight in the component level behaviour is desired, the semi-empirical technique is the most suitable. As mentioned in the study by Dardenne et al. [19], the only two semi-empirical models that do not require geometrical specifications as input are described by Qiao et al. [59] and Winandy et al. [79]. A disadvantage of the study by Quai et al. [59] is that correlations derived from the compressor performance map are required to compute the compressor power input. The model developed by Winandy et al. [79] is limited as it does not account for frequency variation or injection mass flow rate prediction. In the study presented by Dardenne et al. [19], the model of Winandy et al. [79] is adapted to remove these shortcomings. The acquired model shows good accuracy and can be reliably integrated in a thermodynamic system model.

The model developed by Dardenne et al. [19] divides the compression process into nine steps. This is more detailed than the model of Winandy et al. [79], in which the injected mass flow was not accounted for in a separate step, but was combined with the suction mass flow. Also Winandy et al. [79] neglected internal leakage, heat transfer to the screws, a pressure drop at the suction and discharge port and a variation in the rotational frequency. In the model by Dardenne et al. [19], only the pressure drop over the suction and discharge port and the heat transfer to the screws are still ignored. The steps in this model are visualised in figure 2.8 and are:

1. Heating at the suction side (isobaric)
2. Mixing with the internal leakage flow (isobaric)
3. Compression up to the pressure at which the injection port is uncovered (isentropic)
4. Mixing with the injection flow (isobaric)
5. Compression up to the intermediate pressure (isentropic)
6. Mixing with the injection flow (isobaric)
7. Compression up to the adapted pressure (isentropic)
8. Compression at constant machine volume up to discharge pressure (adiabatic)
9. Cooling at the discharge side (isobaric)

In reality, the injection mass flow is not constant but varies with the orbit angle of the screws. The injection mass flow is driven by the pressure differential between the compressed cavity and the injection line. During the injection process, the compression volume decreases. Before the injection port is covered again, the pressure in the cavity might become larger than the injection line pressure. In this case, back-flow will occur. To take this effect into account in the compressor model, two injection steps are included. The mass flow rate at the second injection step can be either negative or positive. This effect is clearly described by Dardenne et al. [19] and is illustrated in figure 2.9. This figure shows that the injection process is simplified, but quantitatively still representative. Both the study by Wu et al. [81] and Moon et al. [51] give a qualitative insight in the phenomena influencing the cycle performance when adjusting the injection line pressure. A key finding is that an optimal (system specific) injection line pressure can be found that maximises the COP. Using the two-stage injection model representation by Dardenne et al. [19], a more accurate estimate of the optimal COP could potentially be achieved. Such an optimization is out of the scope of this study.

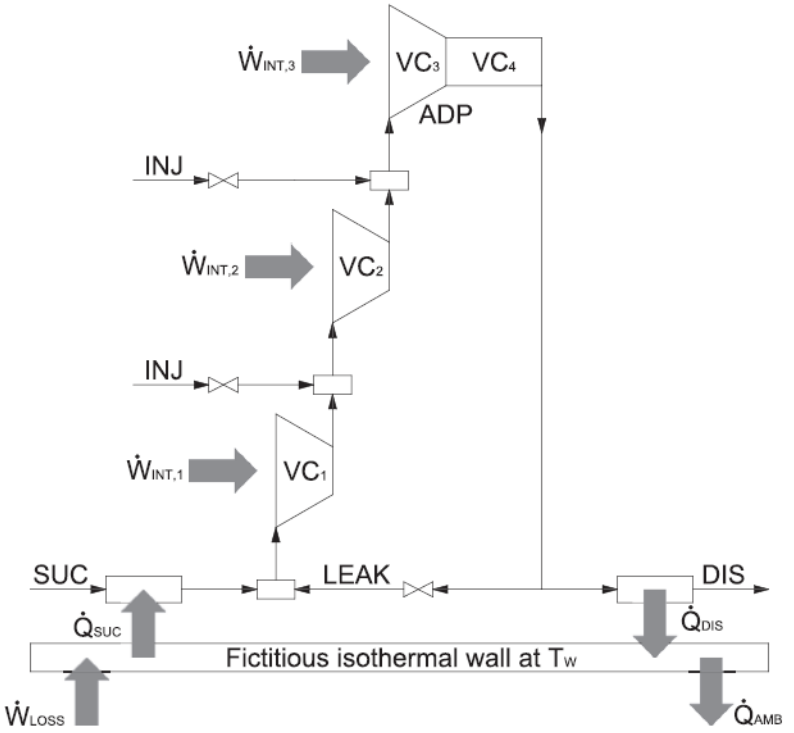

Figure 2.8: Schematic diagram of the compressor model by Dardenne et al. [19]

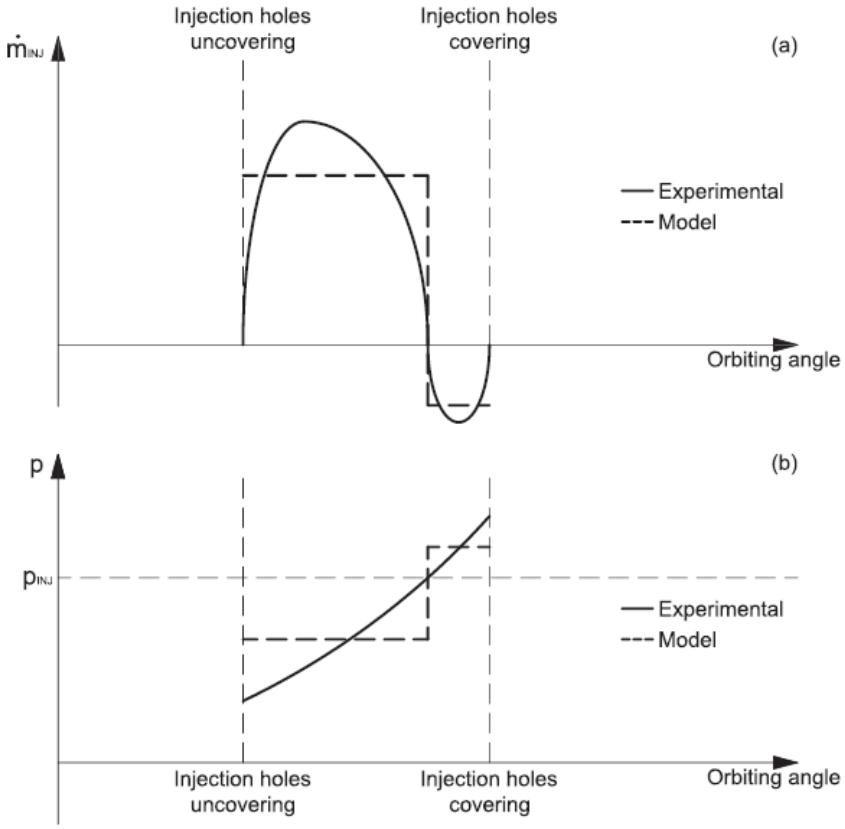

Figure 2.9: Mass flow rate of injection (a) and pressure in the compression cavity (b) as a function of the orbiting angle [19]

2.3. Heat pump dynamics

2.3.1. Previous work

The dynamics of heat pumps have been studied in the past decades by means of modeling and experimental studies. The experimental work is primarily used for validation of the modeling efforts made and based on small scale, domestic heat pumps. The first efforts to develop a full system dynamic model were made in the 70's by MacArthur [17]. Over the years, several dynamic models are presented, as summarised in the literature review presented by Rasmussen [61]. A subdivision in modeling techniques can be identified; the black, gray and white box models. The black box models are fully empirical and therefore system specific. Although suitable for macro analysis, they are not suitable for heat pump design optimization or detailed analysis of component level behaviour. On the other end of the spectrum are the white box models. These models are fully described by the physical laws. In practice, most of the developed models are a mix of both and are therefore called the gray box models.

Even more than for the compressor, as discussed in section 2.2, attention is paid to the modeling of the heat exchangers [78]. This because of the relatively complex physical phenomena that occur in the evaporation and condensation process. Three discretization techniques of the heat exchangers are described in literature; the lumped parameter model, the moving boundary model and the finite volume model. The lumped parameter model describes the heat exchanger as a single volume, or, in case both single phase and two-phase flow regions are present, into multiple volumes. The moving boundary model is an extension of the lumped parameter model, where the volume sizes are dynamic as well. Especially in the early years of heat exchanger model development, these two types of models were the preferred choice because of the relatively low computational power required. Because of the same reason, finite volume models are developed much more in recent years. The finite volume model divides the heat exchanger in many control volumes. This technique is found to be more accurate in describing startup, shutdown and load change dynamics [17].

The first effort in heat pump modeling made by MacArthur was also based on the finite volume method. Other models in which the transient behaviour of heat pumps is studied are presented by, among others, Librado et al. [41], Li et al. [40] and Meesenburg et al. [45]. In the study by Librado et al. [41], the lumped parameter model is applied. Li et al. [40] implemented the moving boundary model, and Meesenburg et al. [45] in their more recent study the finite volume model. Note that none of these dynamic heat pump models, nor the models mentioned in Rasmussen [61], correspond with the cycle layout studied in this report, as presented in figure 2.3. A more relatable study is presented by Qiao et al. [59], in which a flash tank economizer cycle with a vapor injection scroll compressor is modeled.

A follow up study, also by Qui et al. [60], describes the experimental validation of the developed model. In this study, an analysis is presented in which the dynamic behaviour on the component level is discussed. Apart from the study of Meesenburg [45], none of the aforementioned studies is focused on industrial sized heat pumps. A recent study by Kobe Steel [34] does focus on the industrial heat pump discussed in subsection 2.1.3, but is solely experimental.

The PhD thesis by Meesenburg [44] covers the dynamic modeling of an 800 kW heat pump, in combination with experimental validation. This ammonia based, low temperature heat pump is used for district heating. The cycle layout (two-stage) differs significantly from the heat pump studied in this report (single stage). Furthermore, Meesenburg implemented more simple compressor models as no vapour is injected. The main factor limiting flexible heat pump operation was found by Meesenburg to be the risk of vapor formation in the piston compressor suction line during load level changes.

2.3.2. Flexible operation

The share of variable renewable energy is rapidly increasing [68]. Because of the intermittent character, a larger imbalance in supply and demand is expected. With this, the electricity price is also expected to show larger variations. Flexible operation of industrial heat pumps allows to make use of the varying electricity price, and make operation more cost effective. This is a benefit for the end user, as well as for the heat pump manufacturer. The heat pump manufacturer profits from this, because an increasingly interesting investment case will make the heat pump market expand.

The larger imbalance is a problem for the transmission system operator, who is responsible for the grid stability. To balance the supply and demand in the Netherlands within one imbalance settlement period of 15 minutes, the transmission system operator makes use of the automatic Frequency Restoration Reserve [4]. Operators of equipment with a (combined) electrical power of 1 MW and higher can be contracted by Tennet, the Dutch transmission system operator, for this reserve. This can be financially attractive, as mentioned in the whitepaper by Agro Energy [74]. To be contracted, a minimum ramping rate of 10% per minute, for the power range of 1 - 4 MW, and 7% per minute for 4 MW and above is required [3].

2.4. Research facility

2.4.1. Ochsner heat pump

As part of the LowCapex project [1], the previously mentioned steam producing Ochsner industrial heat pump is installed at TNO in Petten. This heat pump will, in future projects, be used for demonstrating flexible heat pump operation. The heat pump, with a thermal capacity of 2 MW, is visualised in figure 2.10. The design is based on the economizer cycle as discussed in subsection 2.1.3. Using this heat pump, steam can be produced up to a temperature of 125°C, from waste heat as low as 40°C. The heat pump is equipped with a VFD to allow stepless control of the compressor speed. Further specifications of the heat pump are covered throughout the report.

Figure 2.10: Ochsner 2 MW Heat Pump [67]

Figure 2.11: Heat pump test rig [67]

2.4.2. Test rig

For dynamic experiments, the heat pump will be connected to a test rig. This test rig is developed for the supply of heat and for the uptake of generated steam, and can thus be used to simulate industrial operation. The test rig consists of a buffer vessel which is partly filled with water. This water is heated and can be used for the supply of low temperature heat to the evaporator. A second, smaller vessel is used for the separation of steam and liquid. The liquid is supplied to the refrigerant condenser, and the generated steam flows back to the separator vessel. The separator after the steam generator is thus not part of the heat pump itself. The water evaporation temperature in the condenser is controlled by the pressure in the separator vessel. The steam from the separator vessel flows back to the buffer vessel and is injected in the liquid. The increase in thermal energy in the buffer vessel is compensated by a water-glycol cooling circuit which transports the heat to the ambient using air cooled heat exchangers.

3

Dynamic model

Building further on the presented problem analysis, the development of the heat pump model is presented in this chapter. First, a brief overview of available modeling environments is given. This is followed by a presentation of the individual heat pump component models. In the concluding section, the simulation setup is discussed.

3.1. Modeling environments

Several software environments are available for the modeling of thermodynamic systems. The most commonly used are Aspen Plus, Simulink and Dymola. Aspen Plus is a chemical process simulator, and therefore not primarily focused on the modeling of refrigerant systems. Simulink is a more generic, on MATLAB based block diagram environment for model based design. A similar alternative is Dymola, which is also used for model based design, but based on the Modelica object oriented language.

The model presented in this study is developed using Dymola, in combination with the commercial TIL library by TLK Thermo [66]. The TIL library is leading in the field of large refrigeration system modeling. This is confirmed by the large number of multinational corporations using the library. The models are ideally suited for the design and optimization of large and complex systems.

3.2. Heat pump model development

In this section, the models of the individual heat pump components are presented. First the compressor model is discussed, followed by the heat exchanger and piping models. The oil separator is assumed to have a negligible effect on the heat pump dynamics and is therefore not included in the model. The calibration and assembling of the component models is discussed in chapter 4.

3.2.1. Compressor

As the TIL library does not include a compressor model with injection, the TIL scroll compressor base class is used as a starting point. On this the model by Dardenne et al. [19] is built, as presented in chapter 2. As mentioned in the previous section, scroll compressor models are suitable for screw compressor modeling, because of their similar working principle. Note that in both the compressor studied by Dardenne et al. [19], as well as in the compressor studied in this model, the electric motor is cooled by the suction gas; a so-called hermetic configuration. This aspect is not integrated in the model by Dardenne et al. [19]. For simplification, this is also not included in the model presented here. The isothermal wall is also left out for simplification, see figure 2.8. The heat loss is assumed to occur in the discharge chamber only, because of the higher temperature. Another difference can be found in the fact that in contrast to the model by Dardenne et al. [19], the pressure drop at the suction port and discharge port is implemented in this study. The thermal capacity of the compressor is neglected. This is common practice in dynamic heat pump modeling, because the dynamic behaviour is hard to predict without measurement data [44]. A schematic representation of the developed screw compressor model is visualized in figure 3.1.

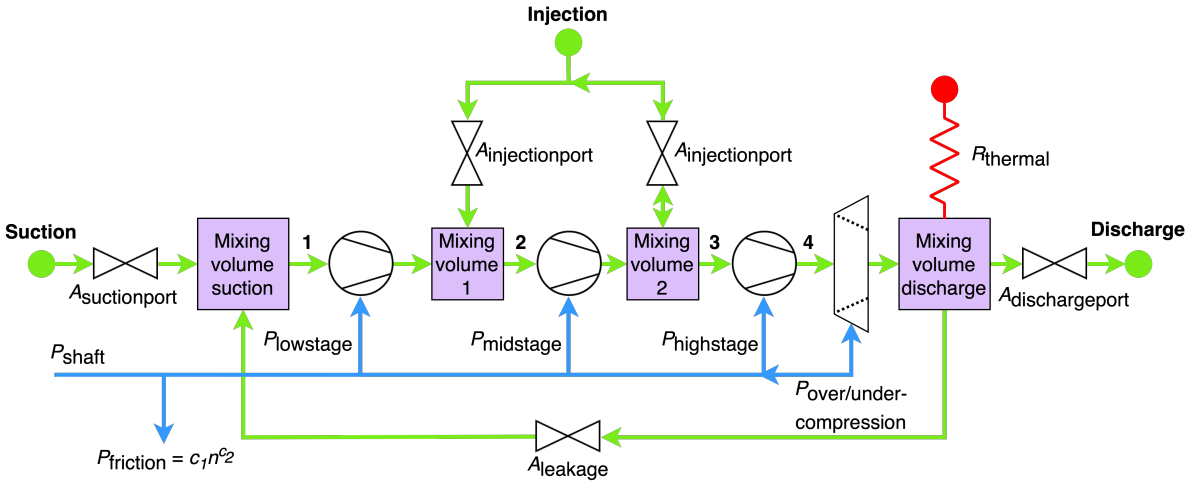

Figure 3.1: Schematic representation of the compressor model

The way the equations are coupled also differs from the model by Dardenne et al. [19] In the current model, the suction and discharge chamber, and the two mixing chambers at the injection ports are modeled as physical control volumes. The derivation of the mass balance over a single volume is presented in equation 3.1. The derivative of the mass with respect to time is written as a function of the pressure and enthalpy. These state variables usually serve as the independent properties in property routines [59]. The right hand side of the equation accounts for the in- and outflow of refrigerant.

$$\frac{dm_{\mathrm{cv}}}{dt} = \sum_{i=1}^{p} \dot{m}_i - \sum_{e=1}^{q} \dot{m}_e \tag{3.1a}$$

$$\frac{dh}{dt}\frac{\partial \rho}{\partial h}\bigg|_p + \frac{dp}{dt}\frac{\partial \rho}{\partial p}\bigg|_h = \frac{1}{\mathrm{V}}\left(\sum_{i=1}^{p} \dot{m}_i - \sum_{e=1}^{q} \dot{m}_e\right) \tag{3.1b}$$

In equation 3.2a-d, the derivation of the implemented energy balance over the mixing chambers is presented. This energy balance is again written as a function of the pressure and enthalpy. The energy rate balance as presented in Principles of Engineering Thermodynamics is taken as a starting point (a) [52]. First the kinetic and potential energy are neglected. As a result, the energy in the control volume equals the total internal energy (b). Taking the partial derivative (c) of the definition of the internal energy, the equation can be written as presented in (d). Note that the volume of the mixing chamber volume does not change. Because no work is done by the control volume, the work term can be excluded.

$$\frac{dE_{\mathrm{cv}}}{dt} = \dot{Q}_{\mathrm{cv}} - \dot{W}_{\mathrm{cv}} + \sum_{i=1}^{p} \dot{m}_i\left(h_i + \frac{v_i^2}{2} + g z_i\right) - \sum_{e=1}^{q} \dot{m}_e\left(h_e + \frac{v_e^2}{2} + g z_e\right) \tag{3.2a}$$

$$\frac{dU_{\mathrm{cv}}}{dt} = \dot{Q}_{\mathrm{cv}} + \dot{W}_{\mathrm{cv}} + \sum_{i=1}^{p} \dot{m}_i(h_i) - \sum_{e=1}^{q} \dot{m}_e(h_e) \tag{3.2b}$$

$$\frac{dU_{\mathrm{cv}}}{dt} = \frac{dH}{dt} - p\frac{d\mathrm{V}}{dt} - \mathrm{V}\frac{dp}{dt} \tag{3.2c}$$

$$\frac{dh}{dt} = \frac{1}{\rho_{\mathrm{cv}}\mathrm{V}}\left(\dot{Q}_{\mathrm{cv}} + \sum_{i=1}^{p} \dot{m}_i(h_i) - \sum_{e=1}^{q} \dot{m}_e(h_e) + \mathrm{V}\frac{dp}{dt}\right) \tag{3.2d}$$

The properties at the in- and outflow of the three compression steps are coupled by the constant entropy and by the change in density with respect to the suction chamber. The latter is defined by the

internal volume ratio Vi. The internal volume ratio of the first compression step, Vi_{ls}, is coupled to the internal volume ratio of the intermediate compression step, Vi_{ms}. This coupling eliminates one unknown parameter and is also implemented by Dardenne et al. [19], as a function of the swept volumes. Dardenne et al. [19] defines the swept volume of the mid stage compressor as the average of the swept volume of the low and high stage compressor. See equation 3.3a-c for the implemented relations. See figure 3.1 for the numbering.

$$Vi_{\mathrm{ls}} = \frac{2}{1 + \frac{1}{Vi_{\mathrm{ms}}}} = \frac{\dot{m}_2 \rho_1}{\dot{m}_1 \rho_2} \tag{3.3a}$$

$$Vi_{\mathrm{ms}} = \frac{\dot{m}_3 \rho_1}{\dot{m}_1 \rho_3} \tag{3.3b}$$

$$Vi_{\mathrm{hs}} = \frac{\dot{m}_4 \rho_1}{\dot{m}_1 \rho_4} \tag{3.3c}$$

For the coupling between the mass flow rates through the suction, discharge, injection and leakage port and the respective pressure drop, equation 3.4 is used [46]. The flow through the port area A is assumed to be adiabatic and isenthalpic. The effects of viscosity and turbulence are neglected, and the expansion factor Y is introduced to account for the compressibility.

$$\dot{m} = AY\sqrt{2\rho(p_{\mathrm{b}} - p_{\mathrm{a}})} \tag{3.4}$$

For the calculation of the mass flow rate, the refrigerant is assumed to behave as an ideal gas. This assumption can not be considered valid. A practical, real gas based equation can be obtained for subsonic conditions by introducing the compressibility factor Z. However, because deviations caused by the ideal gas model will be counteracted when fitting the model parameters, this is not included. The ports are also assumed to have a restricting effect on the flow. This allows to describe the coupling using the model of Saint-Venant and Wantzel, see equation 3.5 [72]. The first equation is applicable at choked conditions, when the pressure ratio over the port is higher than the critical pressure ratio. The second equation is used at subsonic conditions. See equation 3.6 for the calculation of the critical pressure ratio p^*. More details can be found in [46].

$$\dot{m} = \begin{cases} A\sqrt{\gamma p_{\mathrm{a}} \rho_A \left(\frac{2}{\gamma+1}\right)^{\frac{\gamma+1}{\gamma-1}}} & \frac{p_{\mathrm{b}}}{p_{\mathrm{a}}} > p^* \\ A\sqrt{2\rho_A p_{\mathrm{a}} \left(\frac{\gamma}{\gamma-1}\right)\left(\frac{p_{\mathrm{b}}}{p_{\mathrm{a}}}\right)^{\frac{2}{\gamma}} - \left(\frac{p_{\mathrm{b}}}{p_{\mathrm{a}}}\right)^{\frac{\gamma+1}{\gamma}}} & \frac{p_{\mathrm{b}}}{p_{\mathrm{a}}} < p^* \end{cases} \tag{3.5}$$

$$p^* = \left(\frac{2}{\gamma+1}\right)^{\frac{\gamma}{\gamma-1}} \tag{3.6}$$

The mechanical friction loss in the compressor is accounted for by assuming the loss to be a function of the frequency n. See equation 3.7.

$$P_{\mathrm{friction}} = c_1 n^{c_2} \tag{3.7}$$

3.2.2. Heat exchangers

The heat pump consists of two parallel refrigeration cycles. Both cycles are practically identical and can be operated individually. For simplification, the model development presented in this study is only focused on a single refrigeration cycle. In this section, first the evaporator model is presented, followed by the condenser and the economizer model.

Evaporator

The evaporator implemented in the heat pump is a single pass, counterflow shell and tube heat exchanger. In this evaporator, the refrigerant is evaporated on the tube side, while the waste heat water cools down on the shell side. A schematic representation of the model is visualised in figure 3.2. The heat exchanger is mathematically represented by two thermally connected tubes. One tube represents the tube bundle, and the other tube the shell. The tube bundle is made up of m tubes. Two heat transfer phenomena are covered in this tube bundle; convective heat transfer at the inner tube wall and

conductive heat transfer through the tube wall. The second tube model that represents the shell, has a negligible wall thickness and is used to model the convective heat transfer at the outer tube bundle wall. As mentioned in subsection 2.3.1, the finite volume method is the most suitable discretization method. The tube is divided into k different cells in the longitudinal direction. The red arrows show the thermal coupling between the two tubes. Note that by representing the shell and tube heat exchanger in this way, the thermal capacity of the shell wall itself is neglected. This is however not considered a problem, because it will lead to a more conservative determination of the maximum flexibility.

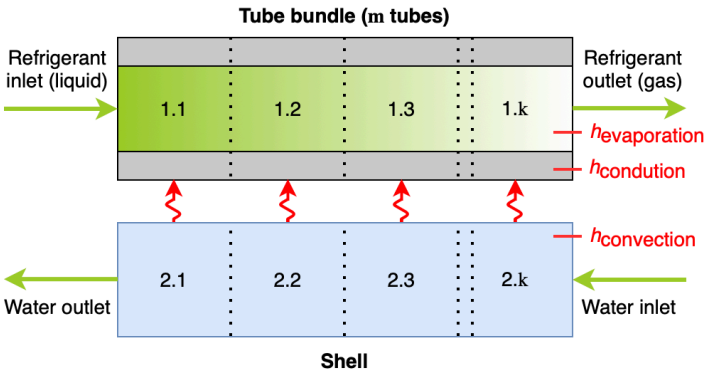

Figure 3.2: Schematic representation of the evaporator model

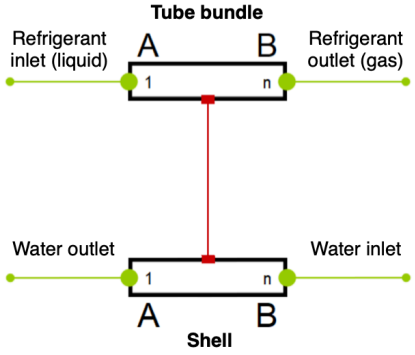

Figure 3.3: Representation of the evaporator model in Dymola

Different heat transfer correlations are used, depending on the flow characteristics. Both single phase and two phase flow can occur in the tubes. For single phase flow, the correlations by Gnielinski, Dittus and Boelter are used and are readily available. The actual correlation applied in each cell depends on the Reynolds number, with the inner tube diameter as the characteristic length. The correlation by Gnielinski is used for the transition region from laminar to turbulent, and part of the turbulent region itself. The correlation by Dittus & Boelter is used for the turbulent region only. See equation 3.8 [47].

$$Nu = \begin{cases} \text{Laminar flow} & 3.6568 & Re_D < 2.3 \cdot 10^3 \\ \text{Gnielinski} & \dfrac{\left(\frac{f}{8}\right)(Re_D - 1000)Pr}{1+12.7\sqrt{\frac{f}{8}}\left(Pr^{\frac{2}{3}}-1\right)} \quad f = (0.790 \ln Re_D - 1.64)^{-2} & 2.3 \cdot 10^3 < Re_D < 1 \cdot 10^5 \\ \text{Dittus \& Boelter} & 0.023 Re_D^{\frac{4}{5}} Pr^{\frac{1}{3}} & Re_D > 1 \cdot 10^5 \end{cases} \tag{3.8}$$

For two phase flow within the tubes, the correlations by Shah and Chen are applied and are readily implemented [18]. The correlation by Chen is limited to vertical tubes only, while the Shah correlation covers both convective boiling coefficient prediction for vertical and horizontal tubes. To make a distinction between the two models, the Froude number (Fr) is used. This number rates the influence of the gravitational force. For Fr < 0.04, the correlation by Shah is applied and vice versa. The hydraulic diameter is used as the characteristic length. More details behind using this distinction can be found in [62]. More background information on the correlations can be found in [18].

The heat transfer coefficient on the shell side is harder to predict. This because the coefficient depends on various geometrical parameters, such as the tube arrangement and the baffle plate design [2]. These parameters are unknown. Because the tube side heat transfer coefficient and the conductive properties through the wall are known, the outer tube heat transfer coefficient will be determined in the calibration step in chapter 4. The order of magnitude of the calibrated heat transfer coefficient is incorrect, due to the use of the wrong heat transfer area. This is a consequence of the model representation as previously presented in figure 3.2. However, because the mass flow rate will not be altered on the shell side (only the temperature), this approach can still be applied.

Because the pressure drops over the shell and the tubes are relatively small, these effects are not

included in the model. This is common practice heat pump modeling [17]. The schematic representation of the model using the TIL Suite library is presented in figure 3.3.

Condenser

Modeling of the condenser requires more creativity. This because of the way the shell and plate heat exchanger functions. A schematic representation is presented in figure 3.4 below. The refrigerant is condensed on the plate side. On the shell side, steam is generated. In this steam generator, the shell side is kept partially filled with water. The water level is actively controlled to keep it constant.

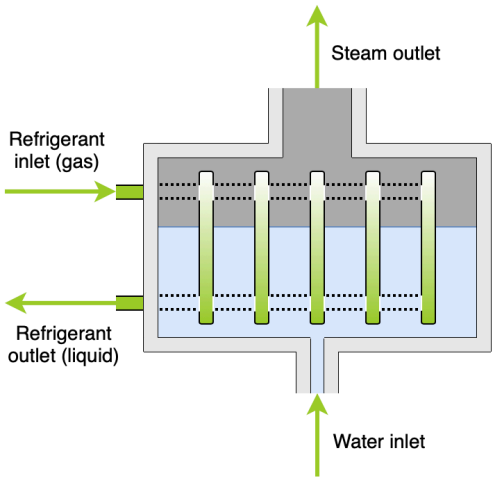

Figure 3.4: Schematic representation of the condenser model

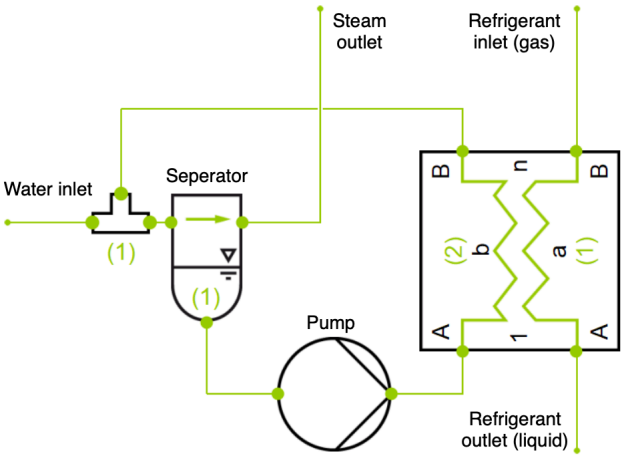

Figure 3.5: Representation of the condenser model in Dymola

Because of this liquid level, it is not possible to use the standard heat exchanger models available within the TIL library. These models do not take into account the effect of a liquid volume on its behaviour. An example of such an effect is the thermal capacity of the liquid. This thermal capacity can have a considerable influence on the dynamics. A solution to describe the behaviour of the shell and plate heat exchanger using readily available components is schematically visualised in figure 3.5. This model consists of a separator, a plate heat exchanger and a pump.

In this model, water enters the separator. The liquid volume in the separator represents the liquid volume on the shell side of the heat exchanger. The liquid is pumped through the plate heat exchanger, at a high rate. As a consequence, the water outlet of the heat exchanger contains only a limited amount of saturated steam. The two phases flow back to the separator inlet. Within the separator, as the name suggests, the liquid is separated from the gas phase, and the steam flows to the steam outlet. Note that because of the liquid volume in the separator, the effect due to the thermal capacity is included in the model. The model also correctly represents the real system's behaviour during a decrease in steam pressure. The condensation of the refrigerant on the plate side is correctly represented by the plate heat exchanger model. The finite volume method is also applied for the discretization method of this heat exchanger.

The heat transfer correlations used on the refrigerant side for single phase flow are the Gnielinski and Dittus & Boelter relation as presented before in equation 3.8 [47]. For two phase refrigerant condensation on the plate side, the correlation by Shah is used [64]. The plate geometry is also taken into account. Apart from the heat transfer resistance due to the wall itself, the surface area increase because of the corrugations is taken into account. The area expansion factor because of the corrugations is calculated using the relation given in the VDI Heat Atlas [2].

On the shell side, the mean liquid flow velocity between the plates due to the inflow of water is estimated to be in the order of a few mm/s at maximum steam generation capacity. Therefore, the applicable heat transfer correlation is assumed to be based on liquid pool boiling, instead of flow boiling. The heat transfer rate in this region depends on the excess temperature, as visualised in figure 3.6.

The definition of the excess temperature ΔT is also included in the figure.

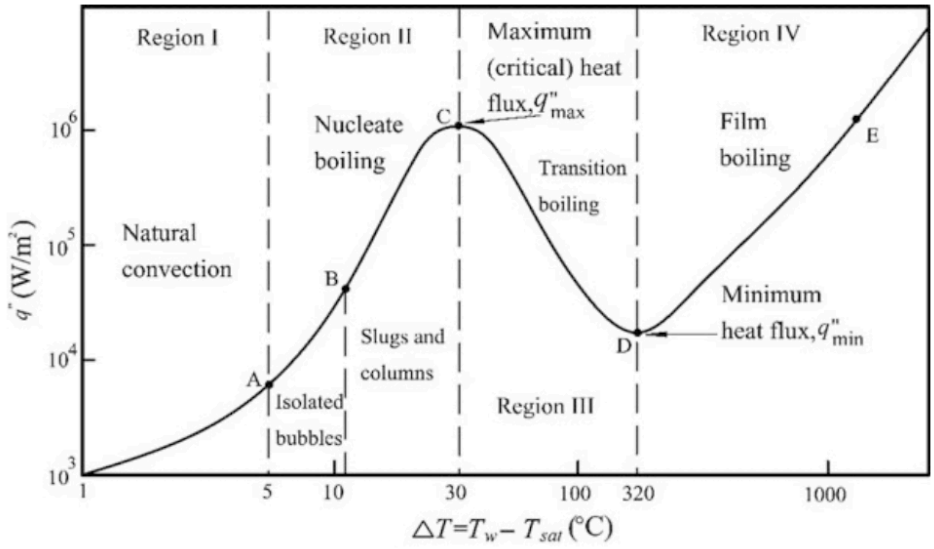

Figure 3.6: Heat transfer regions in pool boiling [24]

The excess temperature is found to be less than 5°C. In this range only the effects of natural convection play a role [24]. Because of the specific geometry, it is hard to accurately predict the heat transfer coefficient. Therefore, the heat transfer coefficient is calibrated based on the manufacturer data. To predict the heat transfer coefficient at deviating operating conditions, a correlation is used. The Rayleigh number at the considered operating conditions is larger than 10^9, meaning the flow is turbulent [47]. For turbulent natural convection along a vertical plate, the heat transfer coefficient can be described using equation 3.9a [16]. This equation is rewritten into equation 3.9b, and implemented in the model. Here, c_3 is used for calibration.

$$Nu = 0.1 Ra_L^{\frac{1}{3}} \tag{3.9a}$$

$$h_b = c_3 \cdot k \cdot \left(\frac{\beta (T_{\mathrm{w}} - T_{\mathrm{bulk}}))}{\nu^2} Pr \right)^{\frac{1}{3}} \tag{3.9b}$$

The fact that the heat transfer coefficient is not a function of flow velocity, makes it possible to use the model representation with recirculating water, as presented in figure 3.5. The vertical water temperature distribution along the plates is assumed to be constant. Also the heat transfer at the top of the plates, where theoretically the water vapor is superheated, is neglected. This contribution is assumed negligible in comparison to the total heat transfer. A situation that is hard to accurately account for in the model without experimental data, is a steam pressure increase. To what extent steam is still generated from the subcooled liquid, because of local saturation, is hard to predict. This is both for the model as well as the actual condenser. Because variations in steam pressure are not studied, as becomes clear in chapter 4, this limitation will not affect the outcomes of this study. Because the pressure drop over the plates is limited (less than 20 mbar), this effect is again not included in the model.

Economizer

The economizer is a brazed plate single pass heat exchanger. On one side, the refrigerant is single phase cooled, while on the other side refrigerant is evaporated. The model used to represent this heat exchanger is the same plate heat exchanger model that is part of the condenser model, see figure 3.5.

The correlations applied to estimate the heat transfer coefficient are described previously. For single phase flow, the correlations by Gnielinski and Dittus & Boelter as in equation 3.8 are used [47]. For two phase flow, a distinction is made between evaporation and condensation. For evaporation, the correlations by Shah and Chen are used [18], depending on the Froude number. For condensation, the correlation by Shah is used [64]. The pressure drop is again neglected.

3.2.3. Expansion valves

The expansion process is assumed to be adiabatic. Because no work is done, and the kinetic energy is assumed to be constant, the expansion process is considered isenthalpic. Also the internal volume of the valve is neglected, because of the much faster dynamics compared to the other heat pump components. For an incompressible fluid, the relation as presented in equation 3.10 can be used to describe the expansion process [46]. Despite the fact that the expanded refrigerant moves into the two-phase region, the incompressibility assumption is still valid. This because the refrigerant after the valve is not in thermodynamic equilibrium. The formation of bubbles is slightly delayed [66].

$$\dot{m} = CA\sqrt{2\rho(p_{\mathrm{b}} - p_{\mathrm{a}})} \tag{3.10}$$

$$\dot{m} = \frac{Kv}{3600}\sqrt{\frac{1000\rho(p_{\mathrm{b}} - p_{\mathrm{a}})}{1 \cdot 10^5}} \tag{3.11}$$

Equation 3.11 is often used in practice to describe the expansion process. The coefficients C and Kv are used to account for the viscosity and turbulence effects, as well as for the difference between the actual and effective flow area. The Kv value is defined as the mass flow rate of water in m^3/h at a pressure drop of 1 bar and a temperature of 20°C. This coefficient is often supplied by expansion valve manufacturers to specify the valve characteristics.

3.2.4. Piping

In practice, different pipes are used to connect the previously discussed heat pump components. To account for the effect of the piping in the heat pump model, the tube model is implemented between the component models. The tube model is also used in the evaporator model, see figure 3.3. Again, the finite volume discretization method is applied. Because the piping is well insulated, the heat transfer between the tube wall and the environment is neglected. The tube wall material and geometrical properties of the actual heat pump piping are taken into account.

The heat transfer models used to describe the heat transfer coefficient at the inner tube wall are already covered: For single phase flow, the correlations by Gnielinski and Dittus & Boelter are used, see equation 3.8 [47]. For evaporation, the correlations by Shah and Chen are used [18], and for condensation the correlation by Shah is used [64]. The pressure drop over the tubes is again neglected.

3.3. Simulation setup

The Dymola modeling environment translates the equations contained in the component models into one Differential-Algebraic system of Equations (DAE). The algorithm that is used to solve this system is the Differential Algebraic System SoLver (DASSL). This solver applies the backward differentiation formula in time [58]. The advantage of using this implicit method is that it is, in contrast to the forward differentiation formula, not limited to a maximum time step in order to remain stable. The DASSL algorithm determines based on the behaviour of the solution the order of the backward differentiation formula and the timestep. The order can range between 1 and 5. At time t, the system of equations is solved by using Newton's method. The DASSL algorithm is considered an efficient solver measured in the number of evaluations. Another advantage of this mature solver is that it is relatively stable over a wide range of models. More details related to the DASSL algorithm can be found in [57] and more details to the implementation can be found in the OpenModelica User's Guide [55].

The heat pump model makes use of the Refprop thermodynamic property library to evaluate the refrigerant properties [39]. The property routines used to retrieve the properties rely on solving relatively complex equations of state. This solving process requires numerical iteration, and is a computationally expensive process. The use of the property routines therefore has a major influence on the total simulation time of the heat pump model [42]. Quantitative details of the simulation times encountered are briefly mentioned in chapter 5. On average, using a time step of 0.1 s, for 4 seconds of simulation time 3 seconds of computational time was required. This does depend on several factors, such as the hardware specifications.

4

Model calibration and validation

In this chapter, the calibration of individual heat pump component models is presented. The compressor model is discussed first, followed by the heat exchanger models. The performance is calibrated using data provided by the manufacturers. After calibration, the components are connected using the tube models and the performance of the full heat pump model is validated.

4.1. Component models

4.1.1. Compressor

The modeled compressor is the Hanbell RC2-930B twin screw compressor with injection port. This compressor has a nominal capacity of 929 m^3/h, at 50 Hz. The internal volume ratio Vi is 3. A set of the most relevant operating conditions is shared with the manufacturer. For each operating condition, Hanbell either directly or indirectly supplied the suction, injection and discharge mass flow rate, as well as the discharge temperature and the compressor power consumption when using refrigerant R1233zd(E). The data supplied by the manufacturer is partly based on experimental results.

The parameters as presented in table 4.1 on page 27 need to be determined to make the compressor model match the actual compressor performance. A tool developed by TLK-Thermo GmbH is able to do this. This tool, ModelFitter [66], is based on an error minimization algorithm. The output parameters of the compressor model that are matched with the manufacturer data are the suction mass flow rate, the injection mass flow rate, the discharge temperature and the power consumption. In the first fitting step, only one single frequency is considered; 50 Hz. A comparison between the manufacturer data and the simulation output after fitting is presented in figure 4.1 and 4.2 below.

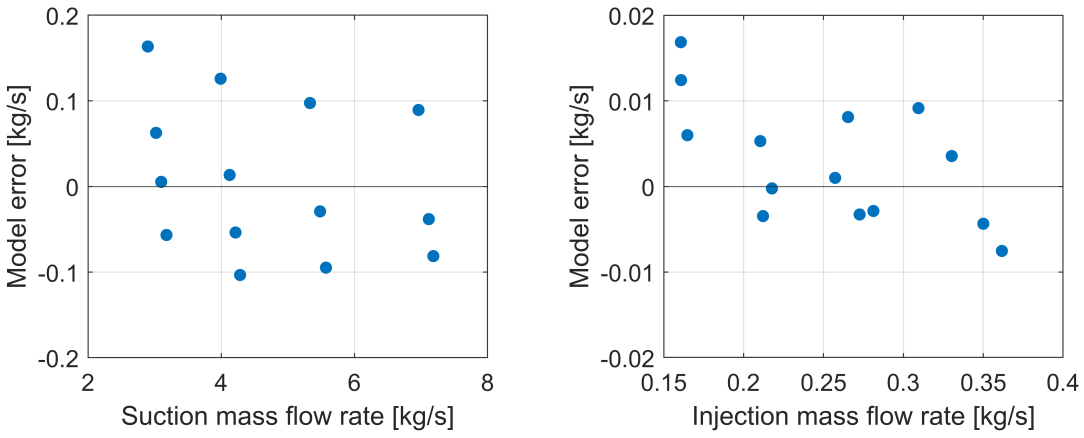

Figure 4.1: Compressor model performance at n = 50 Hz - Suction and injection mass flow

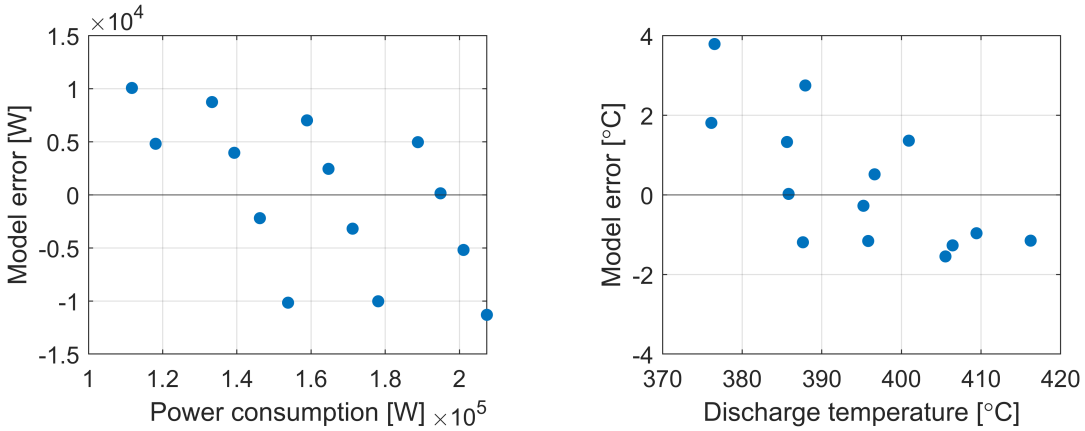

Figure 4.2: Compressor model performance at n = 50 Hz - Power and discharge temperature

From these figures it follows that two output parameters are not well predicted. The injection mass flow rate and power consumption show a maximum deviation of -2/+11% and -7/+9%, respectively. The suction mass flow rate and the discharge temperature are reasonably well predicted, with a maximum deviation of -3/+6% and -0.4/+1%. Instead of random scatter, a pattern can be found in the graphs. The result of further investigation into the cause of the power prediction error is presented in figure 4.3 below.

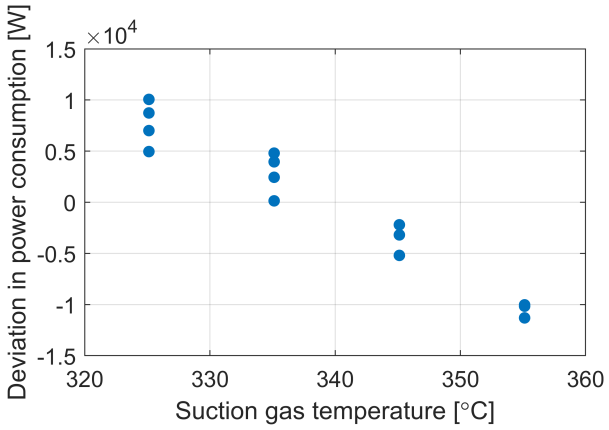

Figure 4.3: Relation between the suction gas temperature and the deviation in the model prediction

From this figure, a trend can be observed between the suction temperature and the power consumption. A possible explanation for this behaviour can be found in the semi-hermetic configuration of the compressor, in which the electric motor is cooled by the suction gas. When the suction gas temperature increases, so will the motor temperature. This temperature increase will cause an increased electric resistance in the motor and therefore a reduction in motor efficiency. It must be noted that because the electric motor is not included in the compressor model, one should be careful in drawing conclusions related to the origination of losses. To include the effect of the electric motor efficiency while also taking into account the influence of the temperature, the compressor model is slightly adjusted, see figure 4.4. The power consumption, at first defined by P_{shaft}, is now given by P_{electric}. The implemented relation is given in equation 4.2 and is assumed to be linear by approximation. The motor losses are converted into heat in the suction chamber.

$$P_{\text{shaft}} = \eta_{\text{motor}}(T_{\text{suc}}) \cdot P_{\text{electric}} \tag{4.1}$$

$$\eta_{\text{motor}}(T_{\text{suc}}) = c_4 + c_5 \cdot T_{\text{suc}} \tag{4.2}$$

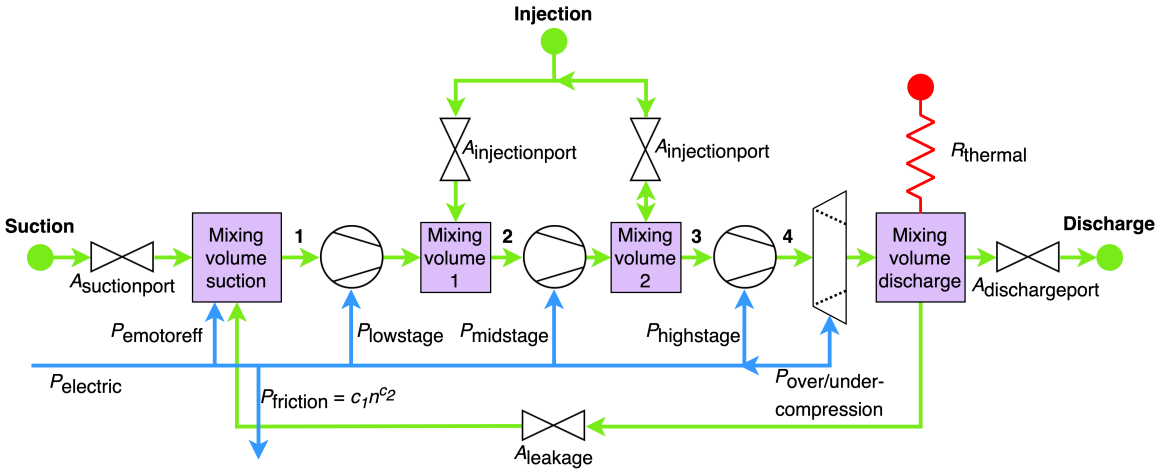

Figure 4.4: Schematic representation of the compressor model with motor losses

The fitting procedure is once more executed, this time by also fitting the coefficients c_4 and c_5 in equation 4.2. The result is presented in figure 4.5 and 4.6 below.

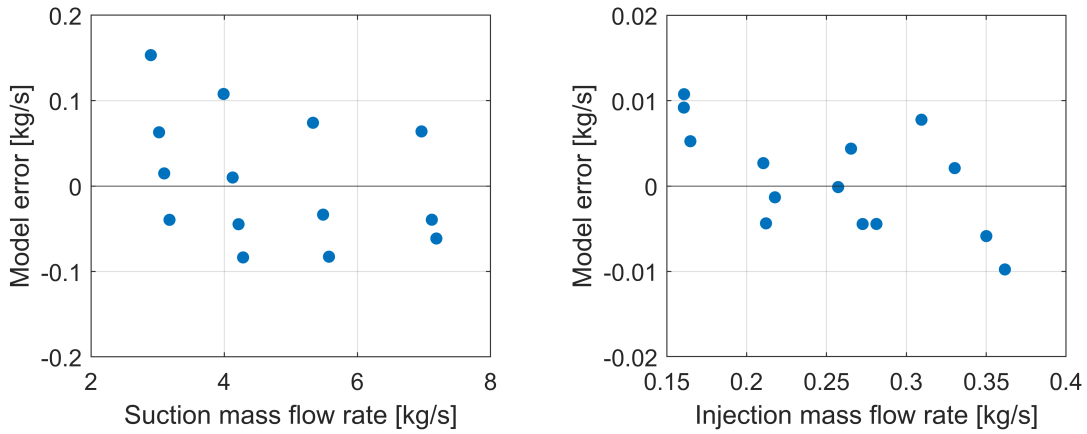

Figure 4.5: Compressor model performance at n = 50 Hz - Suction and injection mass flow

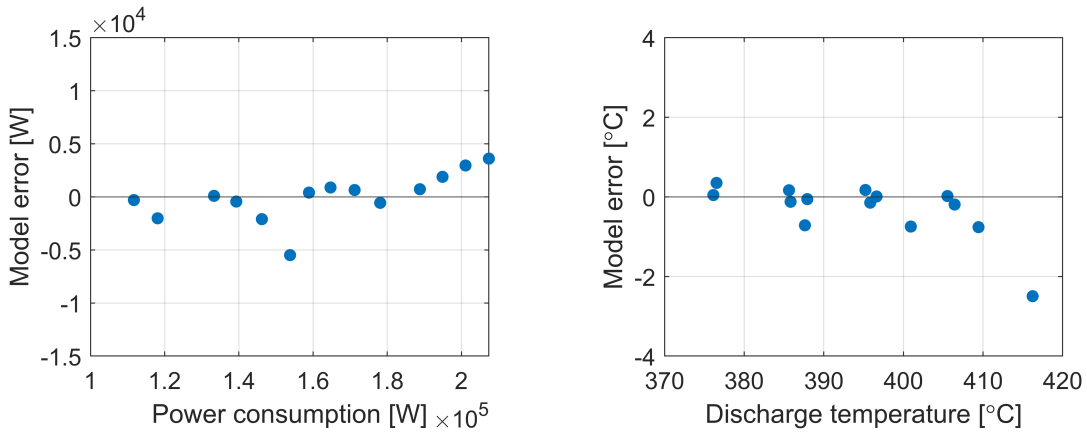

Figure 4.6: Compressor model performance at n = 50 Hz - Power and discharge temperature

From this figure it becomes clear that the model prediction improved significantly. Especially the consumed power is predicted much better: -4/+2%. The deviation in suction mass flow rate has also improved to -2/+5%, and in the injection mass flow rate to -3/+7%. The predicted discharge temperature is still very accurate.

The next step in the fitting process is including the manufacturer data of the compressor performance at a frequency of 25, 33 and 42 Hz. Using the model parameters of the previous fit, the prediction of the mass flow rates is completely off. No clear correlation such as in figure 4.3 is found that explains this behaviour. Fitting the parameters at each frequency independently, does give more insight. From this analysis it follows that:

- The friction loss, as given in equation 3.8 is found to be linear with the frequency. This means the coefficient c_2, see equation 3.7, is equal to one. An analysis on mechanical friction losses in a twin screw compressor are presented in [5] and validate this finding.
- The heat loss at the discharge port is found to be negligible. This could be due to the fact that the compressor has a 175 times larger capacity compared to the compressor studied by Dardenne et al. [19]. When the capacity increases significantly, the area-capacity ratio decreases. Thus the relative effect of the heat loss on the discharge temperature is expected to become smaller. However, in reality some losses are still expected.
- The injection port size should be a function of the frequency in order to obtain an accurate model. A possible explanation for this behaviour could be found in the way the compressor is modeled. Although several physical phenomena are included to describe its behaviour, other aspects are neglected. A relevant phenomena that could be responsible for the found model behaviour is the effect of fluid dynamics. The refrigerant injection process is in reality relatively complex, and is for more insight best studied using computational fluid dynamics. The detailed behaviour of the flow, and thus aspects such as entrainment, might be very different at different frequencies. Again, the difference in compressor size between this study and the study by Dardenne et al. [19] could explain why this effect plays a more dominant role in this study.

The final fitted parameters are included in table 4.1. The model prediction performance is presented in figure 4.7 and 4.8. From these figures, the model can be concluded to be sufficiently accurate for the analysis focused on in this study. The suction mass flow rate and the injection mass flow rate is predicted within -3/+5% and -3/+7%, respectively. The power is predicted within -4/+2% and the discharge temperature within -0.6/+0.3%. Apart from the reasons discussed previously, deviations can also be caused by inaccuracies in the manufacturer data on which the fit is based. More (experimental) research is needed to investigate the origination of errors.

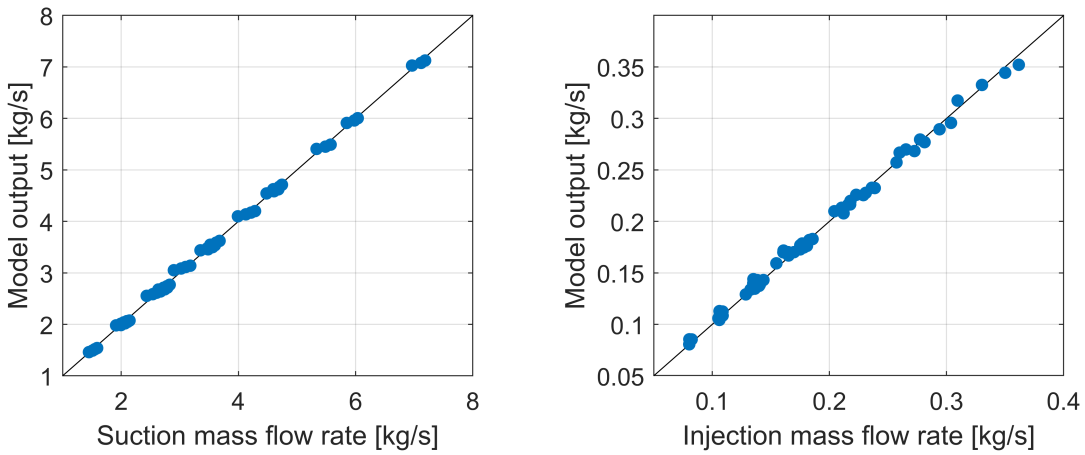

Figure 4.7: Compressor model performance at n = 25, 33, 42 and 50 Hz combined - Suction and injection mass flow

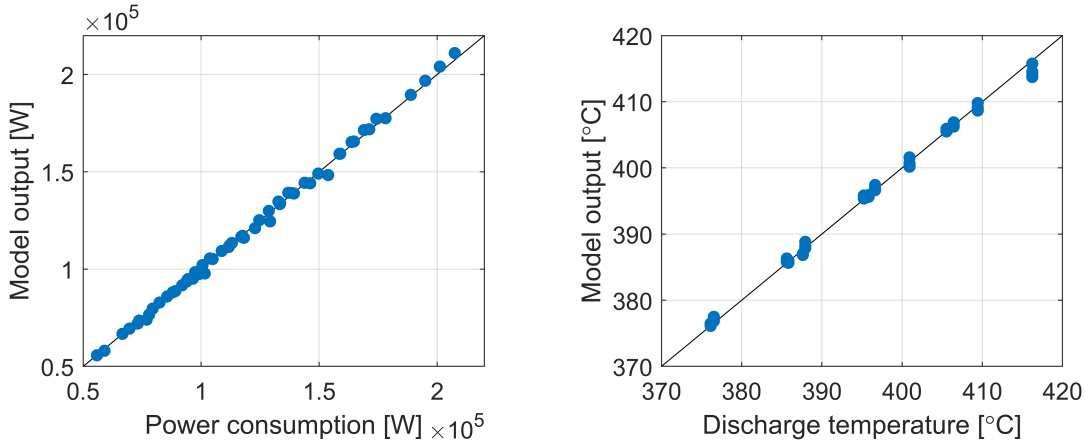

Figure 4.8: Compressor model performance at n = 25, 33, 42 and 50 Hz combined - Power and discharge temperature

Parameter	Description	Value	Unit
A_{suc}	Suction port area	$7.75 \cdot 10^{-3}$	m^2
A_{dis}	Discharge port area	$3.21 \cdot 10^{-2}$	m^2
A_{inj}	Injection port area	$6.06 \cdot 10^{-7} n + 1.15 \cdot 10^{-7}$	m^2
A_{leak}	Leakage port area	$2.81 \cdot 10^{-5}$	m^2
Vi_{ms}	Internal volume ratio midstage compressor	1.34	-
c_1	See equation 3.7	$2.55 \cdot 10^{2}$	-
c_2	See equation 3.7	1.00	-
$h_d \cdot A_{\mathrm{ht}}$	Heat transfer coefficient times area in discharge chamber	-	$\mathrm{W/K}$
c_4	See equation 4.2	$-2.70 \cdot 10^{-3}$	-
c_5	See equation 4.2	1.80	-

Table 4.1: Identified model parameters

4.1.2. Heat exchangers

The evaporator model is calibrated using manufacturer data. This data includes the heat transfer coefficient at given operating conditions, the refrigerant and water volume, and the general dimensions of the heat exchanger. An estimate is made on the number of tubes and the tube wall thickness. Apart from the effect of the wall thickness on the thermal resistance, it also affects the thermal capacity. The heat transfer coefficient on the shell side is, as discussed in subsection 3.2.2, calibrated. At nominal conditions, the heat transfer coefficient is found to be in the order of 10^4 W/m^{2}K. As discussed in chapter 3, the fact that the order of magnitude is not realistic is caused by the incorrect heat transfer area.

The condenser and economizer model both use the readily available plate heat exchanger model. For both heat exchangers the heat transfer coefficient at given operating conditions, the volumes in the heat exchangers and the number of plates is given. For the economizer the plate dimensions are also given, while for the condenser model an estimate is made based on the general dimensions. The plate thickness is calculated to match the plate weight, which is relevant for the thermal capacity. The wavelength and amplitude are calibrated to match the performance. The shell side heat transfer coefficient in the condenser is found to be in the order of 10^3 W/m^{2}K, which can be considered realistic [24].

The volume associated with the water level in the condenser is also given by the manufacturer. The water volume in the separator is kept at this level using a PI controller, see figure 4.11. The actuated variable is the inflow of water, and the measured variable is the water level. In practice, small variations in the liquid level are not expected to affect the heat pump dynamics. The PI controller settings are optimized for stability. The inflow of water is assumed to be at saturated conditions.

As discussed in chapter 2, the most suitable discretization method for dynamic modeling of heat exchangers is the finite volume method. An insufficient number of cells negatively affects the simulation results. The dependency of the results on the grid refinement is therefore used to find the optimal number of cells. The heat pump model presented in the next subsection is used for this study. The model is brought to steady state at reference conditions; 7°C of superheat at both compressor inlets, a steam pressure of 2 bar(a), a waste heat water temperature of 80°C and a compressor frequency of 50 Hz. The superheat at the compressor injection port is found to be particularly sensitive to the number of grid cells. Thus, this parameter is considered suitable to quantify grid refinement effects. The performed grid independence study entails the transient behaviour as well. Note that the number of grid cells is kept the same in all the heat exchangers.

The injection line superheat controller is turned off at a given point, and the expansion valve is closed slightly more in a stepwise manner. The superheat will consequently increase, see figure 4.10. The rise time and the required computational time are presented in figure 4.9, for a different number of cells. The rise time is defined as the time it takes for the superheat to increase by 63% of the total increase measured between the steady states.

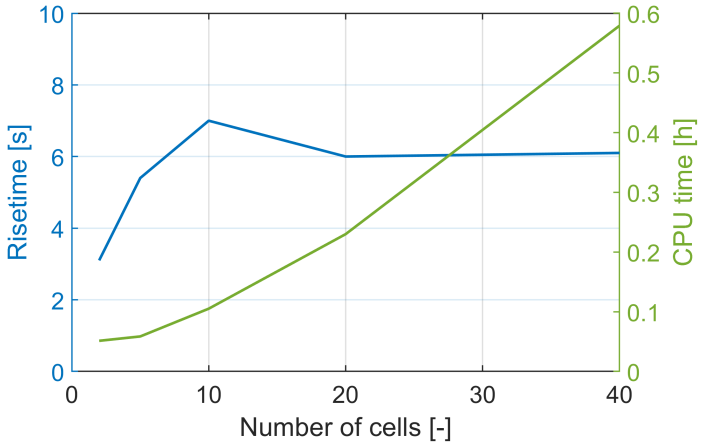

Figure 4.9: Effect of grid size on the model behaviour and computational effort

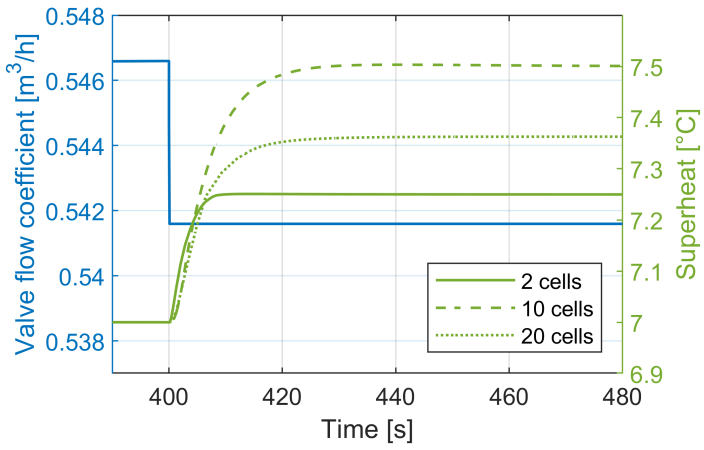

Figure 4.10: Effect of grid size on the system response to a step in the expansion valve flow coefficient

From figure 4.9, it follows that with an increasing number of cells the solution becomes stable. The figure also shows that the computational effort increases exponentially with the number of grid cells. Thus, a compromise is needed between the minimum acceptable model accuracy and maximum computational effort. An optimal compromise is decided to be a total number of 25 cells per heat exchanger. Because the effect of the piping grid size is expected to have a smaller effect on the simulation results, the same grid size is used for these component models.

4.2. Heat pump model

All the individual heat pump components as presented earlier are assembled into the economizer cycle layout discussed in subsection 2.1.3. The dynamic heat pump model is presented in figure 4.11 below. The shell side of the evaporator is connected to a mass flow boundary on the inlet side and a pressure boundary on the outlet side. The condenser contains the previously discussed controlled mass flow inlet boundary. The outlet boundary is also a pressure boundary. This pressure boundary represents the pressure in the steam header to which the heat pump is connected. In practice it is aimed at keeping this pressure level constant. Because steam systems in industrial facilities are often relatively large, fluctuations in pressure are limited. The test rig discussed in chapter 2 is able to simulate this.

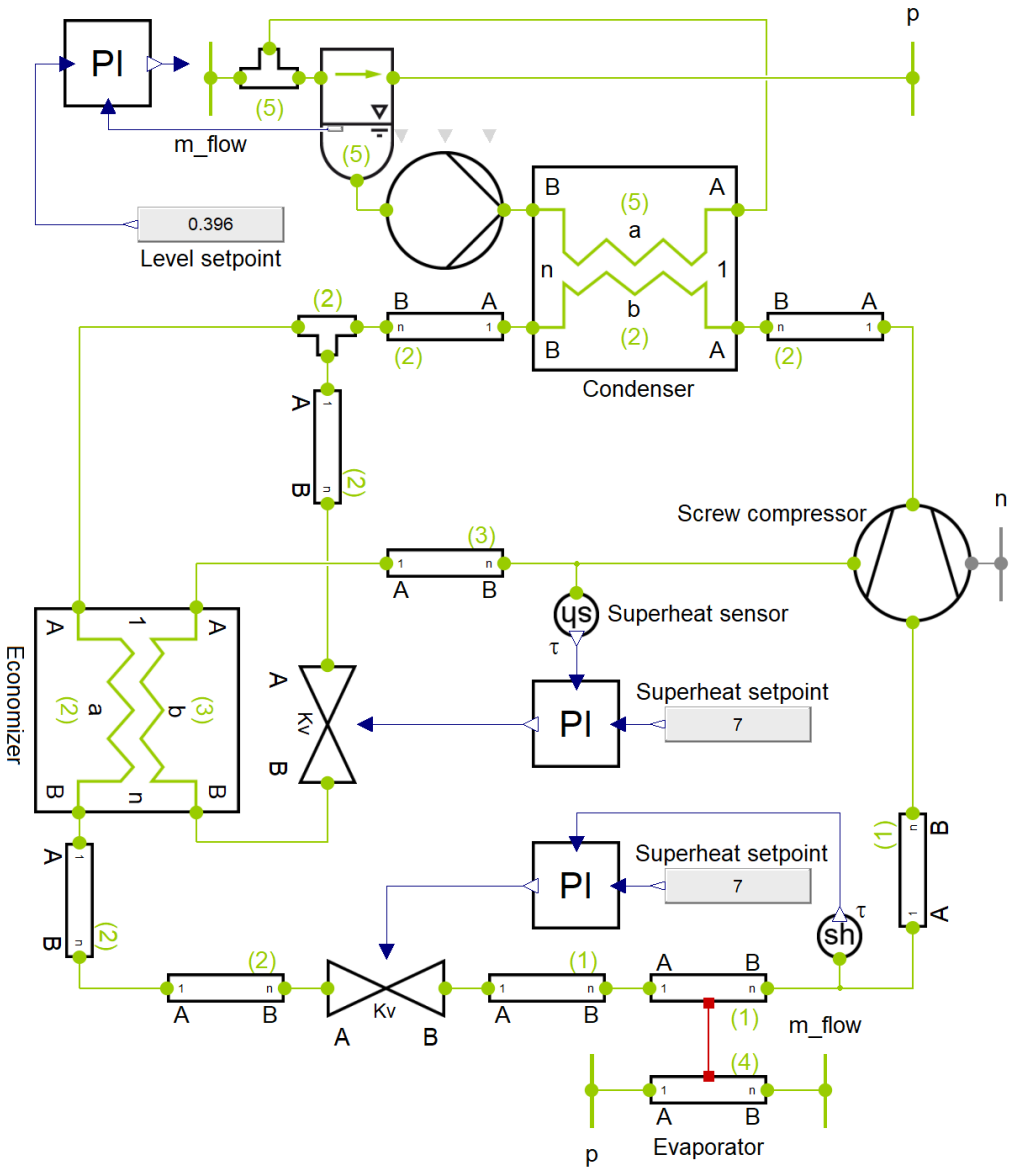

Figure 4.11: Representation of the dynamic model in Dymola

Note that two more PI controllers are implemented. These controllers are used to keep the superheat at a constant value of 7°C. This to ensure no liquid enters the compressors. The goal of these controllers for now is only to bring the system into steady state. Optimization of the control system is discussed in chapter 5.

4.2.1. Steady state operation

The steady state performance of the heat pump is first analyzed using the Engineering Equation Solver (EES) [35]. Both EES and Refprop [39] employ the same reference value for the enthalpy of h_0 = 200 kJ/kgK for saturated liquid at T = 0°C. The conditions at the different state points in EES are used for the initialization of the dynamic model. To compare the model behaviour, the dynamic model is brought into steady state. The steady state performance of the dynamic model was found to show a large offset compared to the analysis in EES. See figure 4.12. It is worth noting that in the dynamic model, the refrigerant is not subcooled after the condenser. This is however required for correct functioning of the expansion valves.

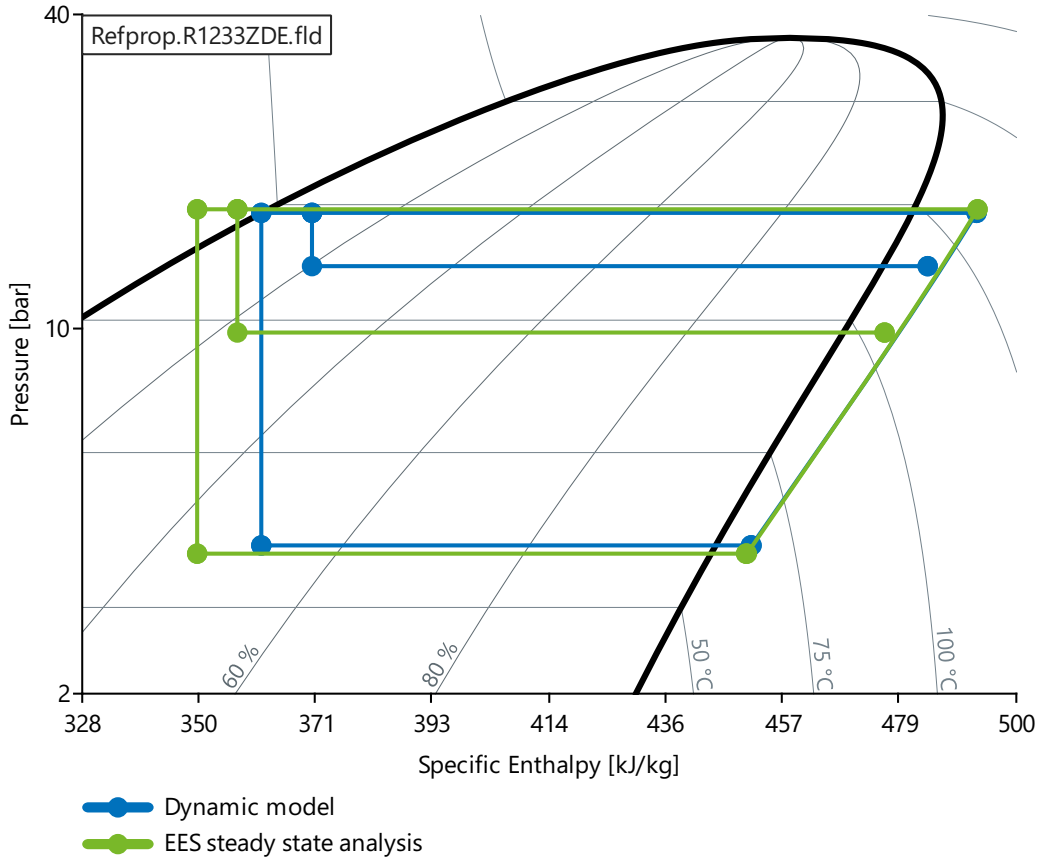

Figure 4.12: Cycle comparison between the dynamic model in steady state and the steady state EES analysis

The observed deviation is found to be related to the refrigerant mass in the system. Because the initialization of the enthalpy distribution in the heat exchangers does not fully correspond with the steady state conditions, the total refrigerant mass in the system deviates. By increasing the refrigerant charge in the model, the steady state performance can be improved until it completely matches the EES steady state analysis.

This effect of the refrigerant charge is found to correspond with findings presented in literature. The subcooling after the condenser is used in practice to adjust the refrigerant charge. In domestic heat pumps, insufficient condenser subcooling might indicate the presence of a leak, as insufficient refrigerant is present [21]. Note that the refrigerant charge affects the heating capacity and thus the COP as well. An optimum COP can be found at a given refrigerant charge. Using less refrigerant, the heating capacity is reduced, while the compressor power consumption remains nearly constant. When the refrigerant charge is increased above the optimum, the heating capacity does increase, but the influence of an increasing compressor power consumption becomes dominant.

The effect of the refrigerant charge on the steady state performance of the heat pump model is visualised in the figures 4.13 and 4.15 below. The refrigerant charge in the dynamic model is calibrated to be 90 kg, which corresponds with the charge in the actual heat pump. With this charge, the heat pump operates at its maximum COP at reference conditions. Note that for off-design conditions, the optimal amount of refrigerant alters. From figure 4.13, it follows that with decreasing waste heat water temperature in the evaporator, the refrigerant charge required to operate at an optimal COP slightly decreases. This corresponds with the experimental results presented by Fernando [25], see figure 4.14. Note that the study by Fernando [25] is focused on a small capacity heat pump. This could explain why the optimum refrigerant charge changes more with the evaporator temperature. For the heat pump model developed in this study, the change in COP is relatively limited when the refrigerant charge changes. Whether the implementation of equipment to make the refrigerant charge variable is financially justified, is case dependent and remains out of the scope of this study.

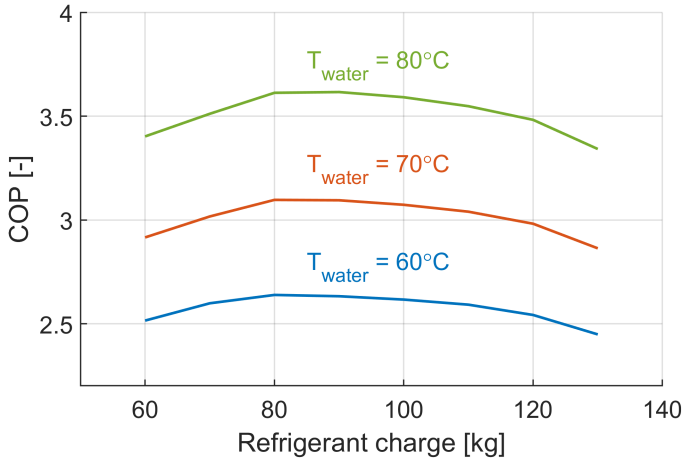

Figure 4.13: Effect of the refrigerant charge on the COP for different evaporator temperatures

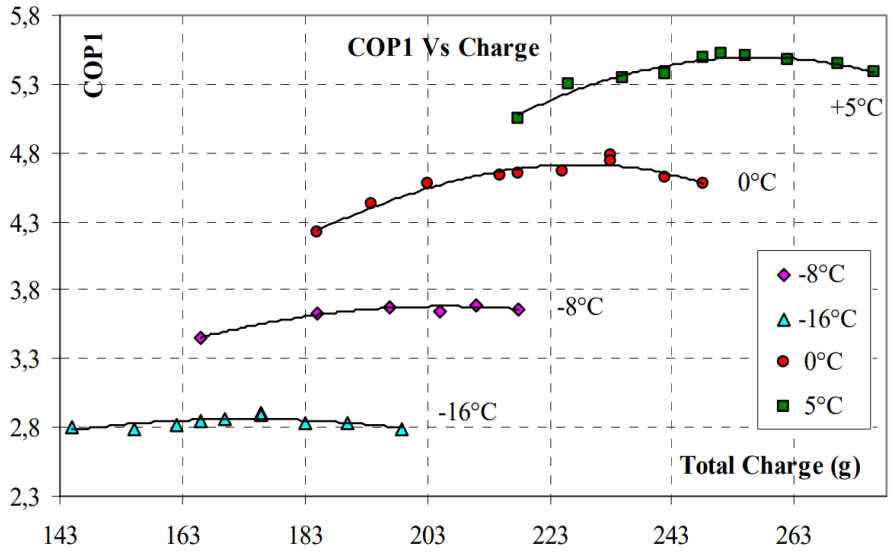

Figure 4.14: Effect of the refrigerant charge on the COP for different evaporator temperatures in a small capacity heat pump [25]

The relation between the refrigerant charge and the subcooling after the condenser is visualized in figure 4.15. From this figure it becomes clear that the subcooling increases with the refrigerant charge. Note that between a charge of 80 and 100 kg the slope of the line is less steep. A similar behaviour is observed in refrigeration systems in literature, see figure 4.16 [77]. Below a charge of approximately 80 kg, the system is undercharged. Above this point, sufficient refrigerant is in the system to have

subcooled refrigerant at the condenser outlet. With a further increase of refrigerant charge, the liquid volume in the condenser will increase. In the region above approximately 110 kg, the increase in pressure in the condenser becomes more significant, causing the degree of subcooling to rapidly increase.

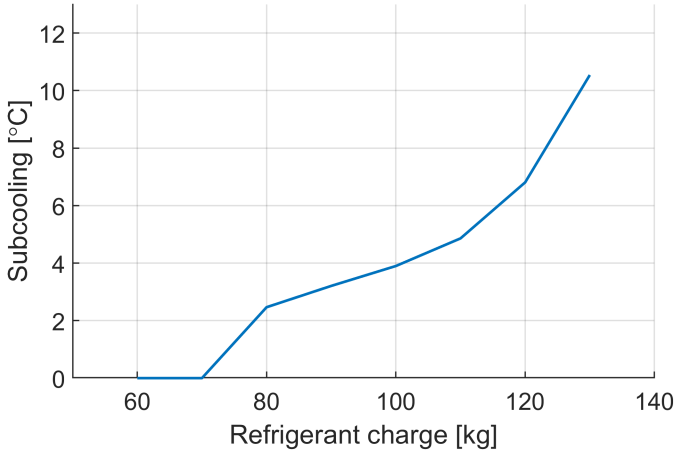

Figure 4.15: Effect of the refrigerant charge on the subcooling after the condenser for T_{water} = 70°C and p_{steam} = 2 bar(a)

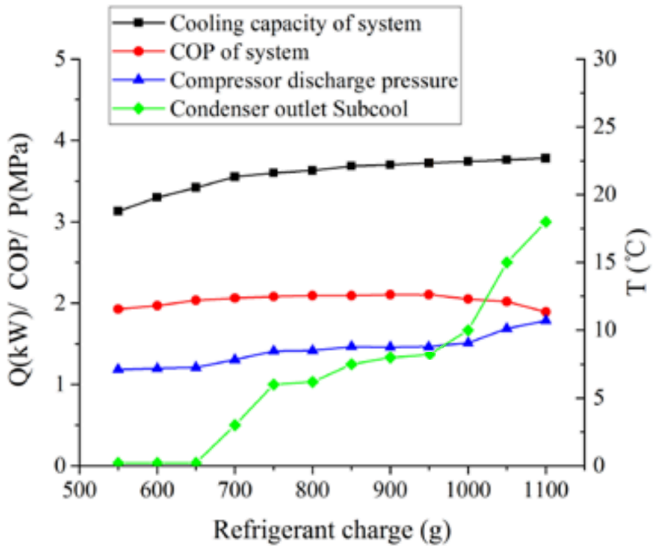

Figure 4.16: Effect of the refrigerant charge on the subcooling after the condenser in an R-134a based air-conditioning system without accumulator [77]

4.2.2. Dynamic operation

Calibration and validation of the dynamics is not possible without experimental data. More details related to this aspect of the heat pump model development are included in Chapter 6.

Aspects accounted for in the model that affect the dynamic behaviour are the volume and thermal capacity of the tubes and the heat exchangers. Aspects that must also be included are the physical time-dependent limitations of the controlled components; the electric motor and the expansion valves. The maximum rate at which the electric motor can ramp up or ramp down is physically limited. In this study, the maximum ramping rate is assumed to be 1 Hz/second. The compressor would thus be able to ramp up to full load conditions (50 Hz) within 50 seconds. As this is expected to be an order of magnitude higher than the overall heat pump dynamics, this is not expected to be a limiting factor. The

same is true for the expansion valves. The magnetic actuators are relatively fast, with a positioning time of less than 2 seconds [65]. This limitation is also implemented in the model.

Another limitation of the compressor is the minimum and maximum compressor speed. The maximum safe compressor speed according to Hanbell is 60 Hz [26]. The minimum safe compressor speed is 25 Hz. Below this frequency, proper lubrication is not guaranteed anymore.

5

Flexible operation of industrial heat pumps

This chapter is subdivided into two parts. In the first part, the focus is on the optimization of the heat pump control system. In the second part, the actual characteristics of flexible heat pump operation are analyzed. Also opportunities for further improvement are identified.

5.1. Control system optimization

5.1.1. Control method

In the actual heat pump, two separate PI controllers are implemented to ensure that the refrigerant gas flowing into the compressor remains superheated at all times. The location of the controllers can be found in figure 4.11. The settings of these controllers are conservative. They are focused on stability and robustness, rather than on responsiveness. Analyzing what the limitations of flexible heat pump operation are using these controller settings is not considered possible. This means that optimization of the control system is needed, where the focus is on both responsiveness, stability and robustness.

As described by Meesenburg [44], different heat pump control methodologies can be distinguished. On/off control is mostly applied in domestic heat pump systems. For larger systems, PID control is deemed a suitable solution. Often multiple subsystems are present, each having their own PID controller. These systems are called SISO control structures (Single Input, Single Output). It depends on the physical coupling between the subsystems whether this is a viable solution. When the coupling is too strong, which means that manipulated variables strongly affect measured variables of other control systems, it might be necessary to adopt more advanced controls. Examples of more advanced control methods are MIMO control (Multi Input, Multi Ouput) and model predictive control.

As mentioned earlier, both electricity response, as well as steam demand response are interesting features for high temperature industrial heat pumps. The control system optimization is focused on steam demand response, because this will also reveal whether electricity price response is possible.

For the studied heat pump cycle, it is unclear to what extent the subsystems are coupled, and thus if the current control system is the most suitable. The relevant manipulated and measured variables are given in table 5.1. The variables on the same row are expected to have the strongest coupling.

	Manipulated variable		Measured variable
u_1	Compressor speed	y_1	Steam mass flow
u_2	Expansion valve evaporator line	y_2	Superheat at compressor suction port
u_3	Expansion valve injection line	y_3	Superheat at compressor injection port

Table 5.1: Manipulated and measured variables

A widely used method to quantify the coupling between subsystems is by calculating the relative gain array (RGA) Λ [56]. The RGA is two-dimensional matrix where the elements represent the ratio between the openloop gain divided by the closed loop gain [80]. In a dynamic system where all the subsystems are fully decoupled, calculation of the RGA yields the identity matrix. In this case, SISO controllers are a suitable solution. The RGA can be calculated using the gain array G, see equation 5.1 and 5.2. See table 5.1 for the definitions of u and y in this study.

$$G = \begin{bmatrix} G_{11} = \frac{\Delta y_1}{\Delta u_1}\Big|_{u_{2,3}} & G_{12} = \frac{\Delta y_1}{\Delta u_2}\Big|_{u_{1,3}} & G_{13} = \frac{\Delta y_1}{\Delta u_3}\Big|_{u_{1,2}} \\ G_{21} = \frac{\Delta y_2}{\Delta u_1}\Big|_{u_{2,3}} & G_{22} = \frac{\Delta y_2}{\Delta u_2}\Big|_{u_{1,3}} & G_{23} = \frac{\Delta y_2}{\Delta u_3}\Big|_{u_{1,2}} \\ G_{31} = \frac{\Delta y_3}{\Delta u_1}\Big|_{u_{2,3}} & G_{32} = \frac{\Delta y_3}{\Delta u_1}\Big|_{u_{1,3}} & G_{33} = \frac{\Delta y_3}{\Delta u_3}\Big|_{u_{1,2}} \end{bmatrix} \tag{5.1}$$

$$\Lambda(G) = G \times \left(G^{-1}\right)^T \tag{5.2}$$

The gain array G can thus be calculated by measuring what happens to an output, when one manipulated variable is changed and the other manipulated variables are kept constant. Translated to the heat pump model, G_{21} for example could be calculated by measuring the superheat at the compressor suction port when the compressor speed is changed, and the expansion valve positions are not changed.

Apart from the manipulated and measured variables, there are two disturbance variables; the waste heat water temperature in the evaporator, and the steam pressure in the condenser. These disturbance variables could influence to what extent the subsystems are coupled. The gain array, and as a consequence the RGA, should thus be calculated for different disturbance values. The model as presented in figure 4.11 is brought into steady state, for each possible combination of compressor speed and disturbance variable value as presented in table 5.2 below.

Waste heat water temperature	Steam pressure	Compressor speed
60°C	1.25 bar(a)	30 Hz
70°C	1.625 bar(a)	40 Hz
80°C	2 bar(a)	50 Hz

Table 5.2: Considered operating conditions (Total of 3×3×3 combinations)

In steady state, the superheat at the compressor inlets is 7°C. At 1400 seconds, the superheat controllers are turned off, and a step on either one of the manipulated variables is performed, while the others are kept constant. Note that there are 27 possible combinations of operating conditions in table 5.2. Running the model three times per combination, to perform a step on each manipulated variable, translates into a total number of 81 simulations. The total simulation time for this batch is 11 hr. For T_{water} = 70°C, p_{steam} = 1.25 bar(a) and n = 40 Hz, the results are presented in figure 5.1 - 5.3 below. The scale on the vertical axis is the same in each graph, to allow for easy comparison.

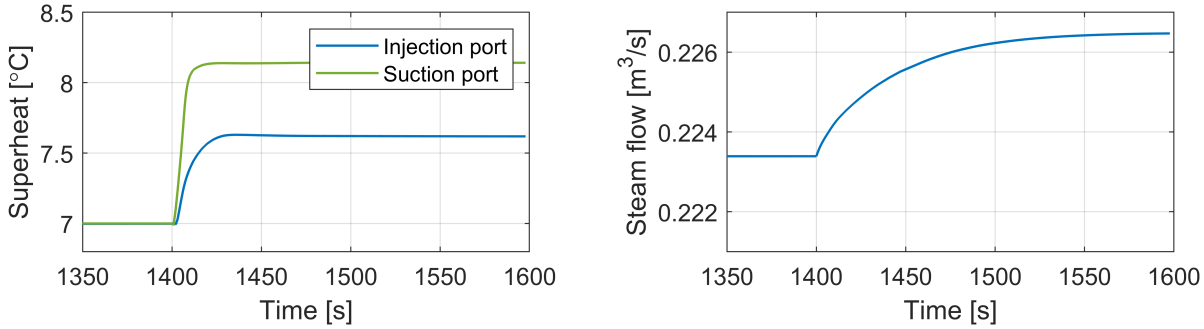

Figure 5.1: System response to a step change in compressor speed (n = 40 → 41 Hz)

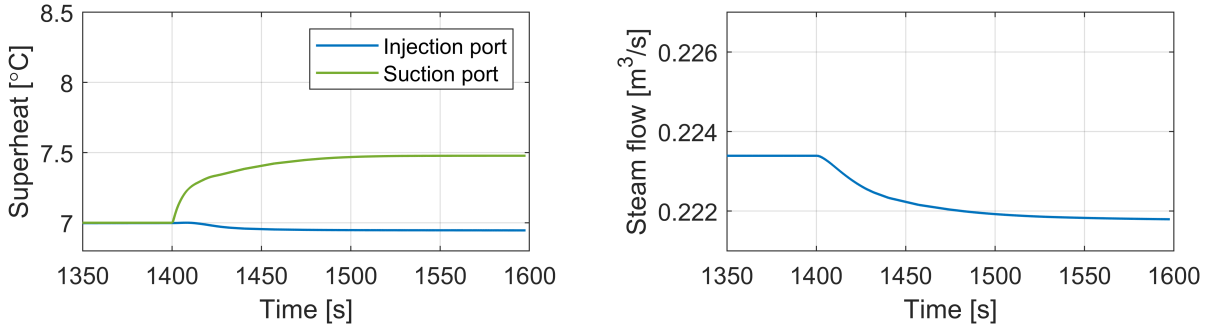

Figure 5.2: System response to a step change in evaporator expansion valve ($Kv_{\text{evaporator}}$ = 3.6678 → 3.6178 m^3/h)

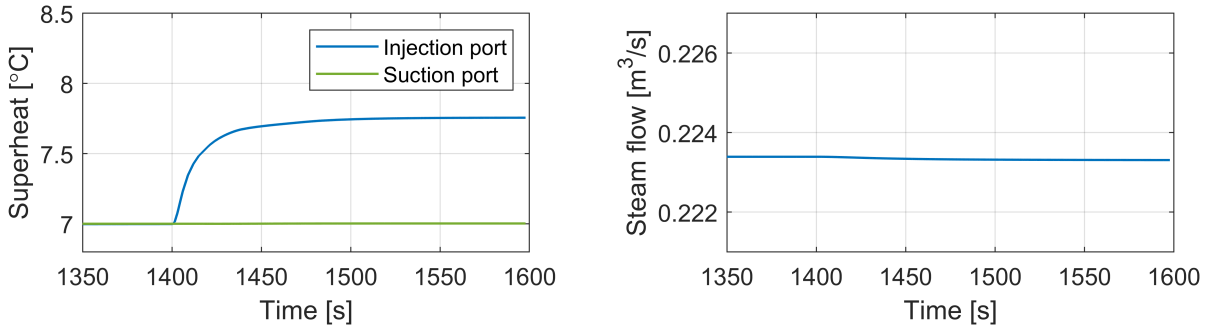

Figure 5.3: System response to a step change in injection expansion valve ($Kv_{\text{injection}}$ = 0.2862 → 0.2812 m^3/h)

From figure 5.1, it follows that the increase in compressor speed strongly affects all the measured variables. In other words; there is a strong coupling. The effect of the evaporator expansion valve on the steam production is also relatively strong, see figure 5.2. This can be expected, because the majority of the refrigerant flows through the evaporator. The superheat at the injection port is not much affected by the evaporator line expansion valve. The expansion valve in the injection line does show a strong coupling with the superheat at the injection port, see figure 5.3. The relatively small refrigerant mass flow rate explains why this valve has no significant effect on the superheat after the evaporator.

The RGA is calculated for each combination of operating conditions. The results of all the 81 simulations are presented in figure 5.4 on the next page. The results of each matrix element are presented in histograms. The most obvious detail is the nearly ideal coupling between the injection line expansion valve and the superheat at the injection port. The fact that this subsystem has a nearly perfect coupling, means that a SISO controller is suitable here. The coupling between the compressor speed and the steam flow is less distinct. Both the compressor speed and the expansion valve upstream of the evaporator have a large influence on the refrigerant mass flow through the condenser, and thus on the steam generation. This explains why the average of the mean top-left and central on-diagonal elements are not close to unity, but are distributed near the center. At nearly all operating conditions, the relative gain on the diagonal is slightly higher than the off diagonal elements. Thus the best pairing of manipulated and measured variables corresponds with the initial hypothesis. In terms of control implementation, SISO control is at first sight not very suitable for control of the steam flow and the superheat at the compressor suction port. This because of the physical coupling between the subsystems.

A second aspect that should be looked at is the coupling in the time domain. For each step response as presented in the figures 5.1 - 5.3, the rise time is analyzed. The rise time is again defined as the time it takes for the measured variable to change by 63% of the total difference between the steady states, which corresponds to the time constant in first order systems. The results are presented in figure 5.5. From this figure it follows that the response delay between the steam flow and the compressor speed is much larger (factor 5) than the delay between the evaporator expansion valve and the evaporator superheat. Because of this, the implementation of two separate SISO controllers for these two systems can be considered feasible [56].

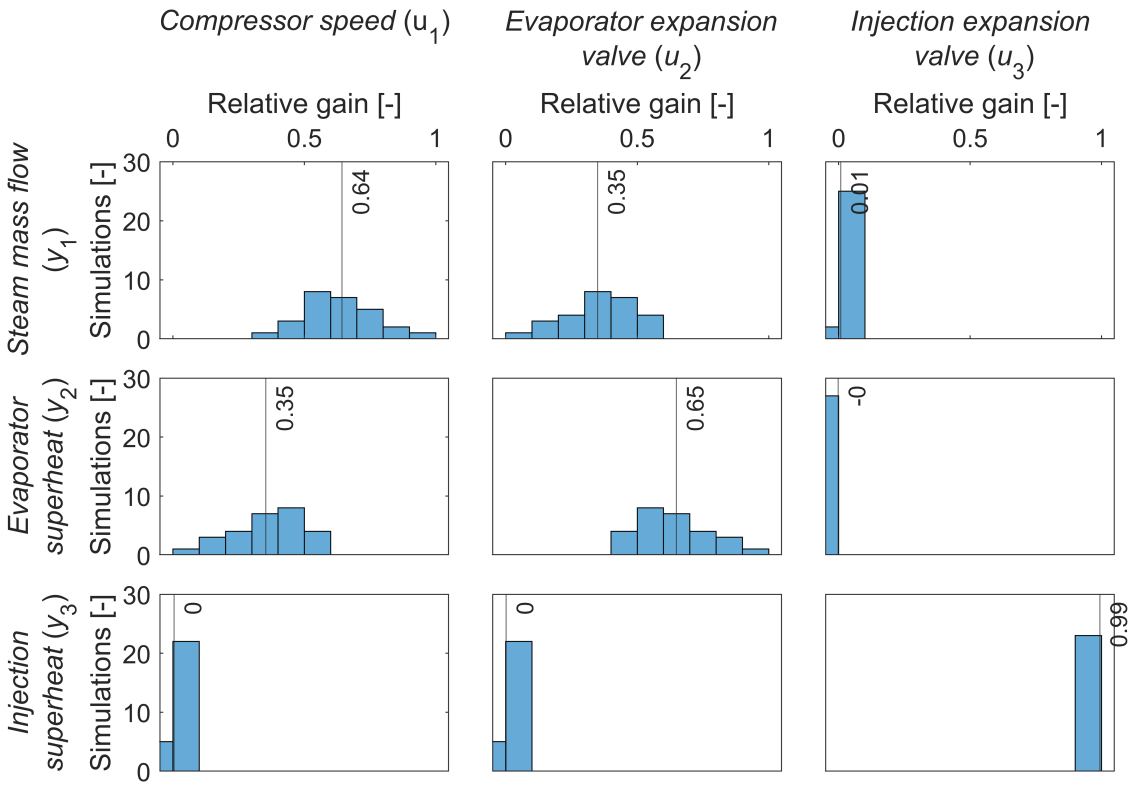

Figure 5.4: Relative Gain Array

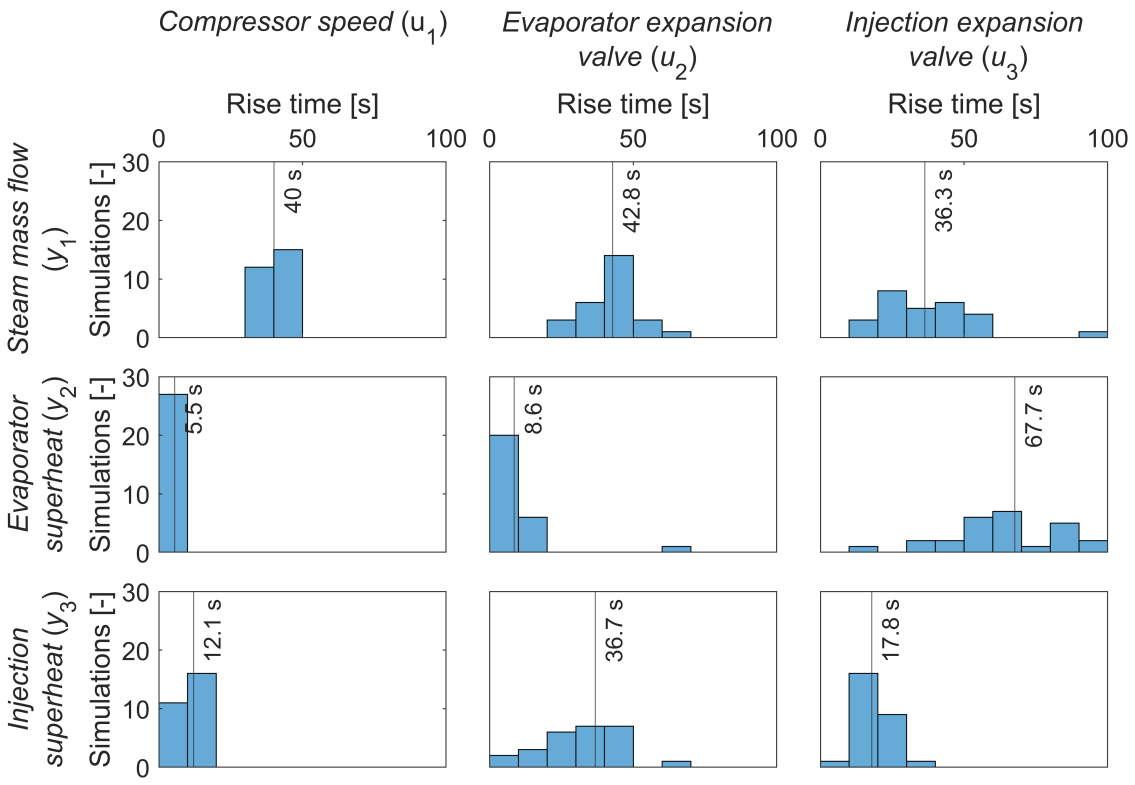

Figure 5.5: Rise Time Array

Because of either physical decoupling, or because of separation in time, the implementation of three SISO controllers can be considered a suitable solution. The implementation of the three SISO controllers is schematically visualized in figure 5.6 below. The most widely applied controllers are the PI and PID controllers. The mathematical description of the controllers is presented in equation 5.3 [13]. For the PI controller, the value of T_d is equal to zero. More details behind the working principle, such as the steady state error elimination by the integral term, are discussed in [13].

$$u(t) = \underbrace{K_p e}_{\text{Proportional action}} + \underbrace{K_i \int_0^t e dt}_{\text{Integral action}} + \underbrace{K_d \frac{de}{dt}}_{\text{Derivative action}} = K_p \left(e + \frac{1}{T_i} \int_0^t e dt + T_d \frac{de}{dt} \right) \tag{5.3}$$

Whether the derivative action - acting as a kind of brake or dampener on the control effort - is required, is case dependent. Because the controlled subsystems in the heat pump have a non-integrating character, a PI controller might satisfy. This is however without taking higher order or nonlinear effects into account. To be able to select the most suitable controller type, both types will be compared.

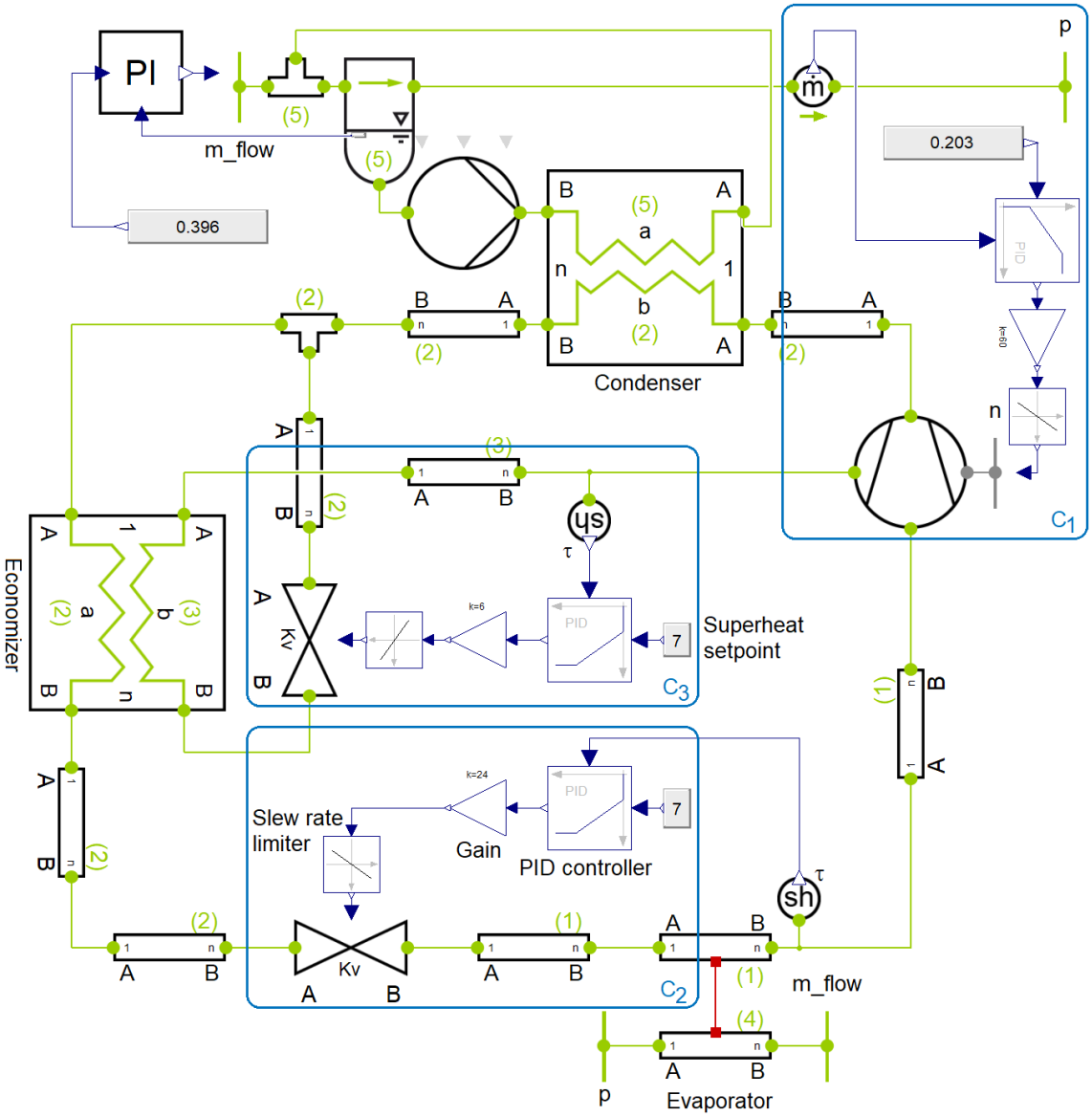

Figure 5.6: Representation of the dynamic model in Dymola with SISO control structure

5.1.2. Controller tuning

In order to use the controllers, the values of the so-called controller settings must be determined. Several different methods for controller tuning can be applied, which can be categorised in trial-and-error, feature based and analytical methods. Feature based methods are based on features of the process dynamics that are easy to obtain experimentally [75]. An example of an analytical method is direct pole placement. Because features of the process dynamics can be easily obtained using the heat pump model, the feature based method is applied. The most widely known method is the Ziegler-Nichols step response method and is developed in 1942. Although a classical method, a disadvantage is the very aggressive tuning result which often results in the need for further refinement [75].

Nowadays, controller tuning most often relies on more advanced, automated tuning algorithms. The basic principle is similar to the Ziegles-Nichols method, but more features are taken into account by the algorithm, and the user has more control. In this study, the advanced tuning algorithm developed by MathWorks is used [31]. The control settings need to be optimized for responsiveness, but should still be conservative.

System identification

In order to apply this tuning method, the process dynamics must be identified. A problem which is not yet touched upon, is the fact that the system is nonlinear in its nature. The system is not expected to have unstable equilibrium positions. Also, close to one operating condition, the system is assumed to behave close to linear. To analyze whether the behaviour can be best described by a first or second order model, two models are fitted on the step response data presented in subsection 5.1.1. The fitted models are the so-called First and Second Order Plus Deadtime models (FOPDT & SOPDT). For the fitting procedure, the MATLAB System Identification Toolbox is used [30]. Because the data obtained in subsection 5.1.1 is used, the same set of 27 different operating conditions is analyzed.

The system identification on the step response of the superheat at the injection port is presented in figure 5.7 below. The temperature and time offset are removed. From this figure, it becomes clear that the model can to a large extent be described by the FOPDT model. However, fitting the SOPDT model achieves a higher fitting performance for this, as well as the other analyzed step responses. The fact that the fitting performance is not perfect can be caused by the presence of higher order or nonlinear effects. Because the systems are best described by the SOPDT model, this description will be used for the tuning of the controllers. The use of the SOPDT model is in literature described to yield better PID tuning results for heat exchanger temperature control systems, compared to the use of a FOPDT model [50].

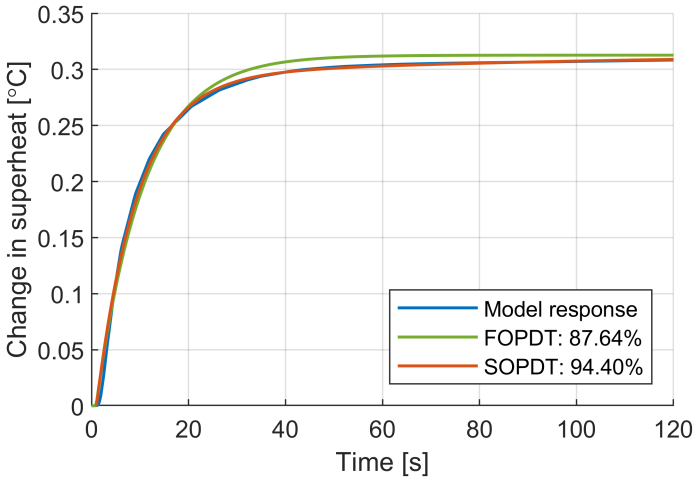

Figure 5.7: Fitting performance of a FOPDT and SOPDT model on the injection line superheat step response

Tuning parameters
As mentioned previously, the PID tuning algorithm by MathWorks is used [31]. This tuning algorithm takes into account the closed loop stability, the robustness and the performance. The robustness is measured by the gain and phase margin, required to allow for modeling errors and variations in system dynamics without having the system to become unstable. By default, the phase margin is 60°. The performance depends on what the goal of the controller is. A distinction can be made between reference tracking and disturbance rejection. By default a balance between these two goals is sought. However, for each of the heat pump SISO controllers one specific goal can be identified. The superheat controllers need to reject any disturbance, while the steam flow controller needs to track the reference signal. The reference signal is in this case the steam demand.

From the step response analysis presented in subsection 5.1.1, the subsystem behaviour is found to depend on the operating conditions. Therefore, the controllers are tuned using the aforementioned settings at each considered operating condition. Both a PI and PID controller are tuned to allow for comparison. For now, the focus will be on the PID controller type. The ratio between the highest and lowest found proportional gain K_p is presented in table 5.3, for the control systems C_1, C_1 and C_1 as presented in figure 5.6.

	C_1	C_2	C_3
$\frac{\max(K_p)}{\min(K_p)}$	2.20	8.66	2.76

Table 5.3: Ratio between the highest and lowest proportional gain K_p

Because of the small range in tuning parameters for controller C_1 and C_3, the mean value of these parameters will be used. For controller C_2, this range is relatively large. To make sure the selected tuning parameters will not cause unstable behaviour at any operating condition, a conservative approach is required. Looking at the subsystem, the effect of the expansion valve on the evaporator superheat has a delay. This delay is expected to be related to the evaporator volume and the mass flow rate. Therefore, for lower compressor speeds the delay is expected to be larger. A larger delay is expected to have a negative effect on the maximum proportional gain. The effect of the compressor speed on the proportional gain is analyzed and visualized in figure 5.8 below.

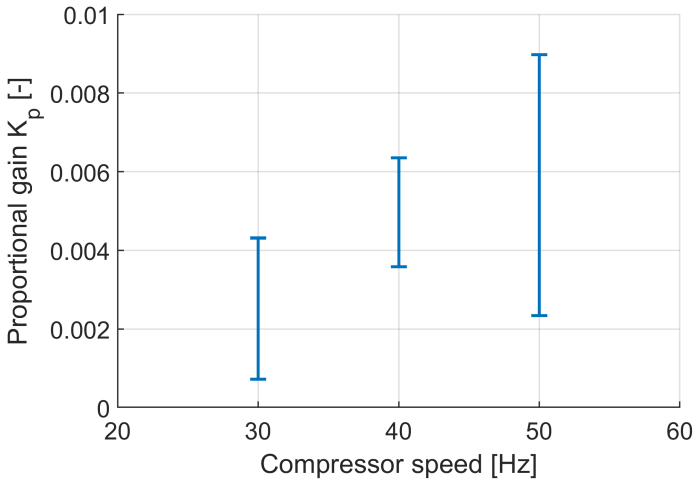

Figure 5.8: Distribution of the proportional gain K_p, sorted by the compressor speed

This figure confirms that the maximum proportional gain is lower at lower speeds. For a conservative approach, the mean gain of the values at 30 Hz only is selected. The final parameters are presented in table 5.4. A comparison between the performance of the PI and PID controllers is presented in figure 5.9. In this simulation, the steam flow demand is varied from 0.327 to 0.205 kg/s, which at steady state

		K_p	T_i	T_d			K_p	T_i	T_d
PI	C_1	6.66	19.5	-	PID	C_1	9.21	38.9	0.66
	C_2	0.00279	4.86	-		C_2	0.00289	4.20	2.61
	C_3	0.00132	14.8	-		C_3	0.00141	10.6	3.34

Table 5.4: PI and PID tuning parameters

corresponds to a compressor speed of 50 and 30 Hz, respectively. First the demand is reduced over a period of 200 seconds, while consequently the demand is increased over a period of 60 seconds. The superheat at the injection and evaporator port are used to compare the effect of the controller type on the superheat. The superheat at the injection port is found to be affected more by the disturbance, see figure 5.9. From the figure it becomes clear that the performance of the PID controller exceeds the PI controller performance. At 820 s, the superheat shows a larger deviation in the PI controlled process. At 1410 s, the refrigerant state even briefly moves into the two-phase region. The performance difference between the controllers can be attributed to the fact that with the introduction of the derivative term, the use of a more aggressive gain becomes possible, especially for controller C_1. See table 5.4. The use of the derivative term also allows to tune the controller better for a specific goal. This can be seen by the reference tracking performance of the steam flow, where the PID controlled process shows almost no overshoot. Summarized, use of the PID controller is the preferred choice. It must be noted that in practice the PI controller is also used [12]. For this two main reasons are identified:

1. No high disturbance rejection is required; for example in industrial heat pump systems that are designed to run in steady state only, for prolonged periods of time;
2. The derivative term makes the controller prone to adverse effects caused by measurement noise. This can however be counteracted by the use of a low-pass filter [13].

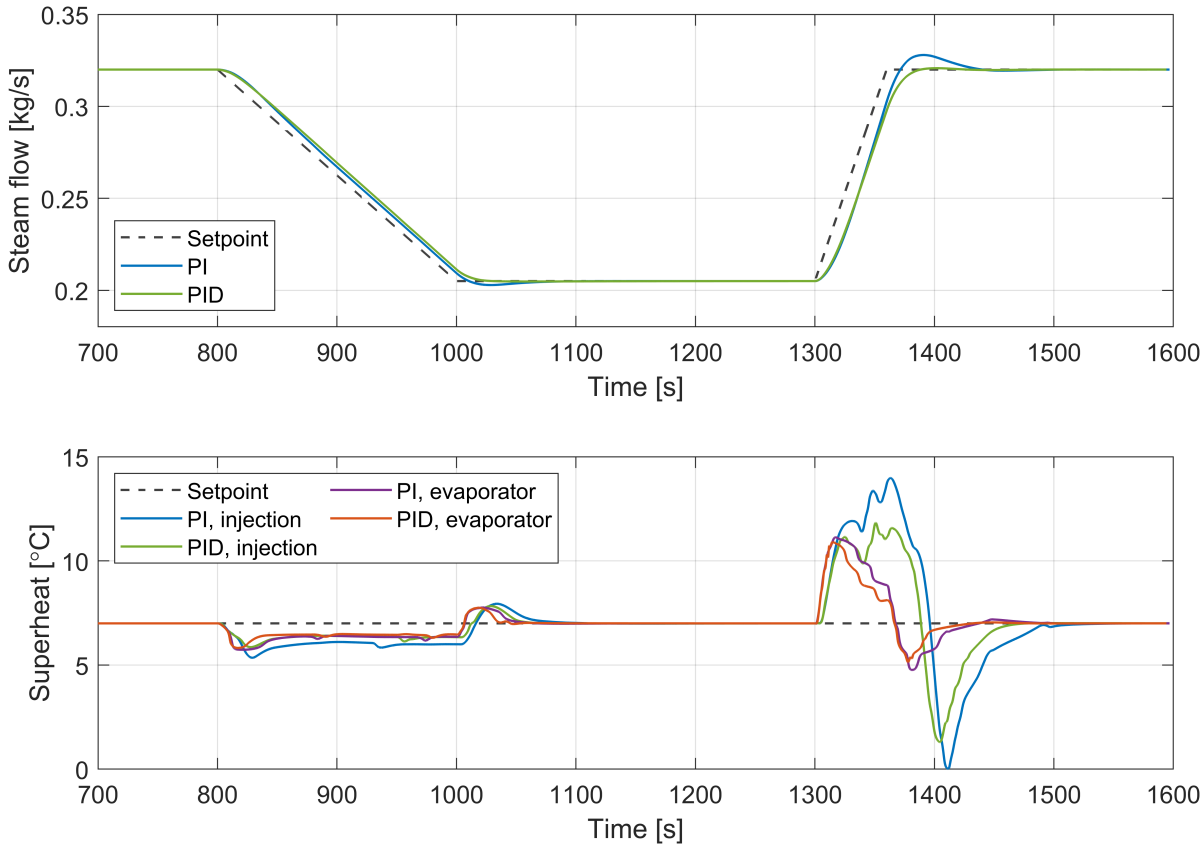

Figure 5.9: Comparison between PI and PID control, at T_{water} = 80°C and p_{steam} = 2 bar(a)

5.1.3. Robustness

Although the simulation result presented in figure 5.9 is only valid for one operating condition, it does give insight in the robustness and stability of the controllers. From this figure, the controllers can be concluded to operate in a stable fashion up to steam demand increase rate that corresponds with 20 Hz/min. However, this insight is limited to a constant waste heat water temperature. To analyze the effect of a simultaneous change in waste heat water temperature and steam demand, three cases are analyzed. The first is a change in steam demand only, the second is a change in waste heat water temperature only, and the third is a simultaneous change. The injection port superheat during all three cases is visualised in figure 5.10.

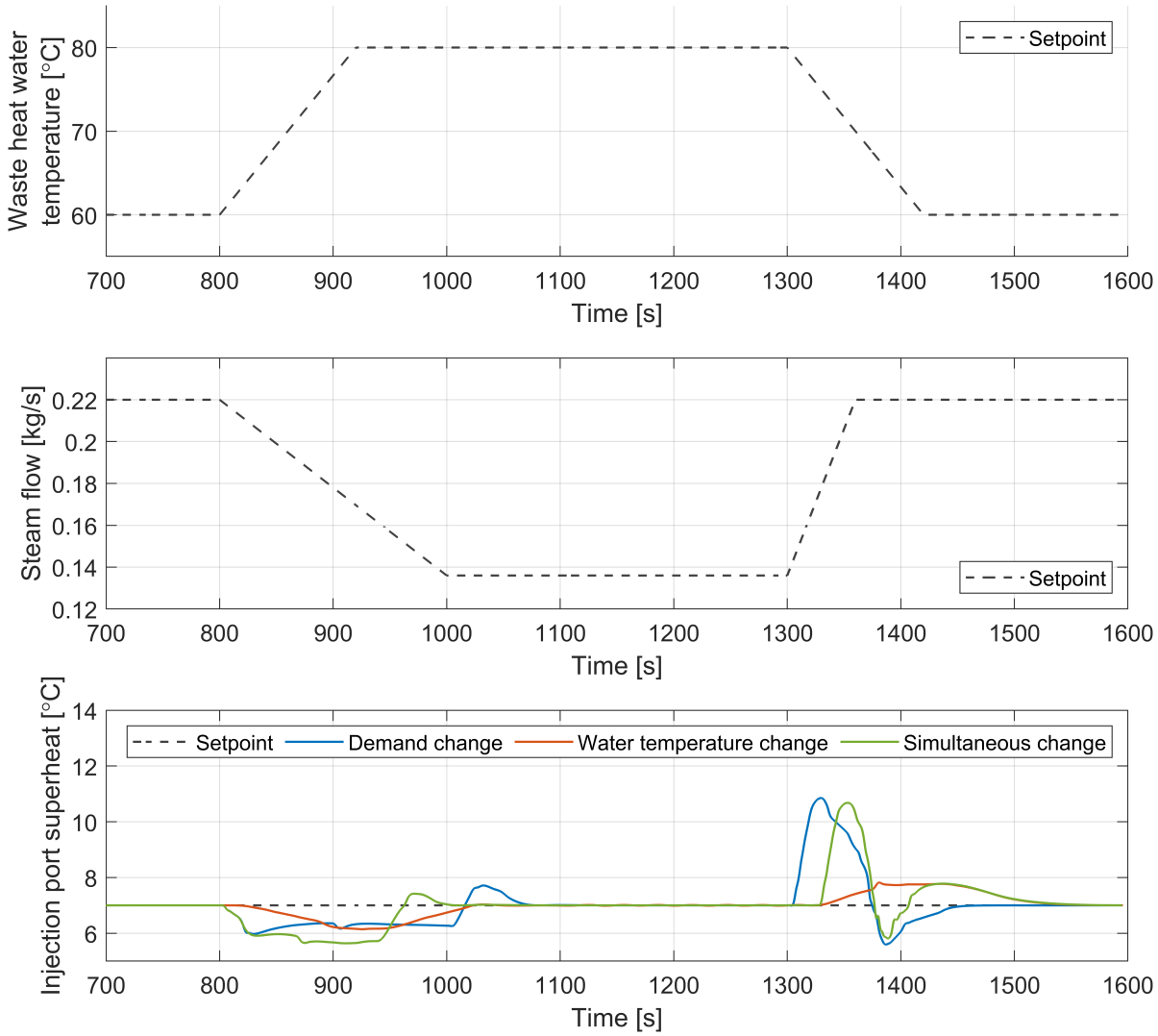

Figure 5.10: Robustness test by varying the steam demand and waste heat water temperature - either independent or simultaneously - for p_{steam} = 2 bar(a)

The combination of ramping the waste heat water temperature up and the compressor speed down is studied, because both decrease the superheat. In the simulation where both effects are combined, the effects do not amplify each other; the decrease in superheat is less than the sum of the independent effects. It can thus be concluded that also for a simultaneous change of steam demand and disturbance variables, the control system shows a robust behaviour.

Looking further into the behaviour of the heat pump, it can be observed that the steam flow demand tracking capability is still reasonable, see figure 5.11. However, because the PID controller is optimized for this goal, the disturbance effect of the waste heat water temperature is clearly visible. As to whether

a more balanced tuning approach is needed depends on the frequency at which waste heat water temperature fluctuations will occur in the industrial setting. Note that from approximately 950 s, the steam flow does not decrease any further. This is caused by the minimum compressor speed of 25 Hz. In this particular case, the default anti-windup compensation feature of the Modelica Standard Library [23] PID controller prevents excessive overshoot after saturation of the compressor speed.

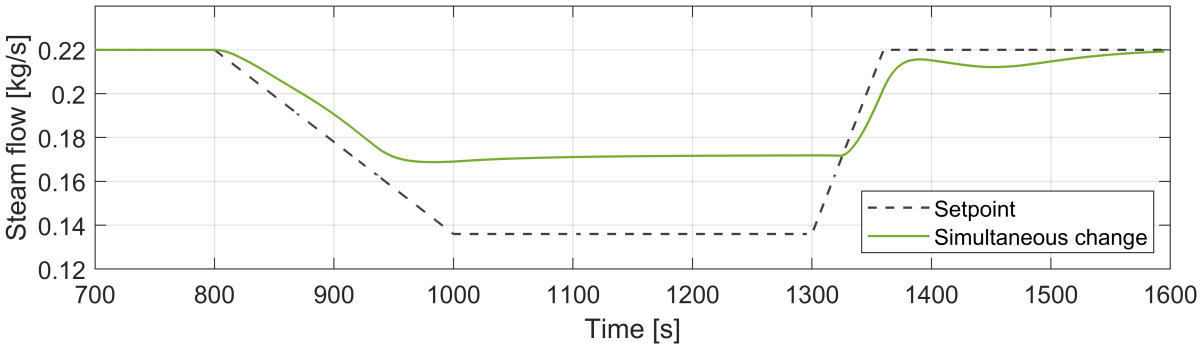

Figure 5.11: Steam demand reference tracking during simultaneous change in steam demand and waste heat water temperature for p_{steam} = 2 bar(a)

5.1.4. Control system improvement

Despite the proven robustness and performance of the implemented control system, there is still room for improvement. The most ideal behaviour one could aim for is no disturbance in the superheat, independent of the ramping rate, and a perfect steam flow demand tracking. Three methods to improve the control system will be discussed, along with a qualitative estimate of the increase in performance.

Gain scheduling

A method to tackle the varying optimal tuning parameters for different operating conditions is so-called gain scheduling. This technique boils down to making the controller settings a function of the operating conditions. Because the ratio between the smallest and largest gains is less than ten, gain scheduling is not expected to yield a significant improvement [66].

Cascade control

Cascade control is a control method which relies on using multiple measured variables for one system, instead of only one. This method is beneficial when the different sensors have different time scales. Cascade control is therefore expected to be particularly suitable for the control of superheat. The amount of superheat is in fact a function of the pressure and temperature. The step response presented in figure 5.3, is further analyzed in figure 5.12 below.

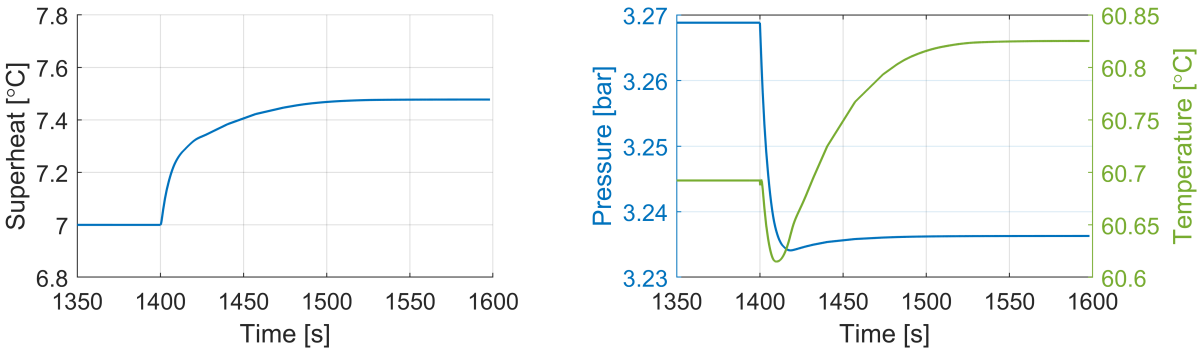

Figure 5.12: Injection port superheat, pressure and temperature response to a step change in injection expansion valve ($kv_{\text{injection}}$ = 0.2862 → 0.2812 m^3/h) at T_{water} = 70°C, p_{steam} = 1.25 bar(a) and n = 40 Hz

From this figure it becomes clear that the pressure level responds much faster to actuation of the expansion valve than the temperature. The implementation scheme of the cascade control method is visualized in figure 5.13. Note that in practice implementation of this control method will will not require the installation of additional equipment, as both a pressure and temperature sensor will already be present for the calculation of the superheat. More details regarding this technique can be found in [56].

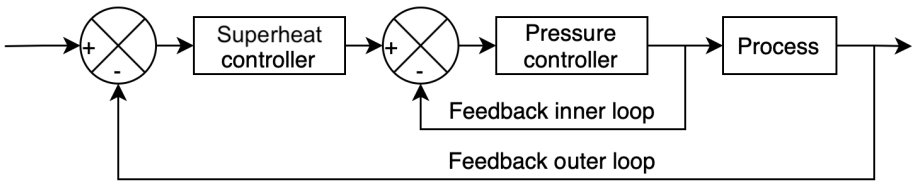

Figure 5.13: Cascade control implementation scheme. Adapted from [37]

Feedforward control

A third considered method is the implementation of feedforward. Feedforward can be implemented in a PID feedback control system in two different ways; for reference tracking and for disturbance rejection. The idea of feedforward is that the control system does not wait for a disturbance to affect the measured variable, but the disturbance is forcing a control variable response immediately. As described in [13], this can improve the controller performance significantly. Note that this control strategy can be combined with the cascade control structure described previously. So-called 'ballistic' feedforward, where no feedback is used at all, is not considered a suitable solution. The system would not be able to react to external disturbances, and the disturbance signal would need to become a processed signal itself based on multiple disturbance variables. The feedforward control system for disturbance rejection, together with a single loop feedback control system, is visualized in figure 5.14 below. For reference tracking purposes, instead of a disturbance measurement, the reference signal is used together with a feed forward gain. Because of the delay in the superheat control systems, implementation of this technique is considered the best first step in further improving the system performance.

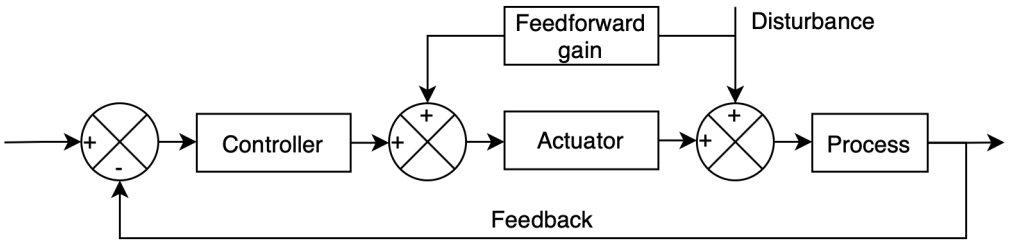

Figure 5.14: Feedforward with feedback control implementation scheme (disturbance rejection). Adapted from [37]

To analyze the potential, the feedforward control structure is implemented on the most limiting injection flow superheat controller. As mentioned previously, disturbance rejection is the main priority of these controllers. The disturbance variable that is most linearly related to the input signal of the expansion valves in steady state is the compressor speed. This can be expected, as the compressor speed primarily dictates the mass flow rate through the heat pump circuit. The feedforward gain G_{ff} can be calculated by dividing the controller output by the compressor speed in steady state, see equation 5.4.

$$G_{\mathrm{ff}} = \left.\frac{u_3}{n_{\mathrm{compressor}}}\right|_{\mathrm{Steady\ state}} \tag{5.4}$$

The position of the expansion valve in steady state does not purely depend on the compressor speed, but also on the steam pressure and the waste heat water temperature. These relations are however not so strong as the relation with the compressor speed. The latter is visualized in figure 5.15.

The feedforward gain is selected to be the mean of the feedforward gains, that follow from all the

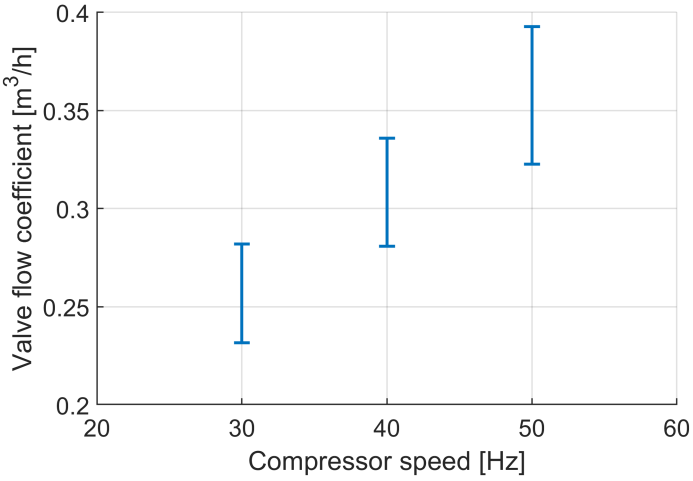

Figure 5.15: Relation between the steady state injection line valve flow coefficient and the compressor speed

considered operating conditions. For a clear performance comparison the same simulation as presented in figure 5.9 is used. The result is presented in figure 5.16.

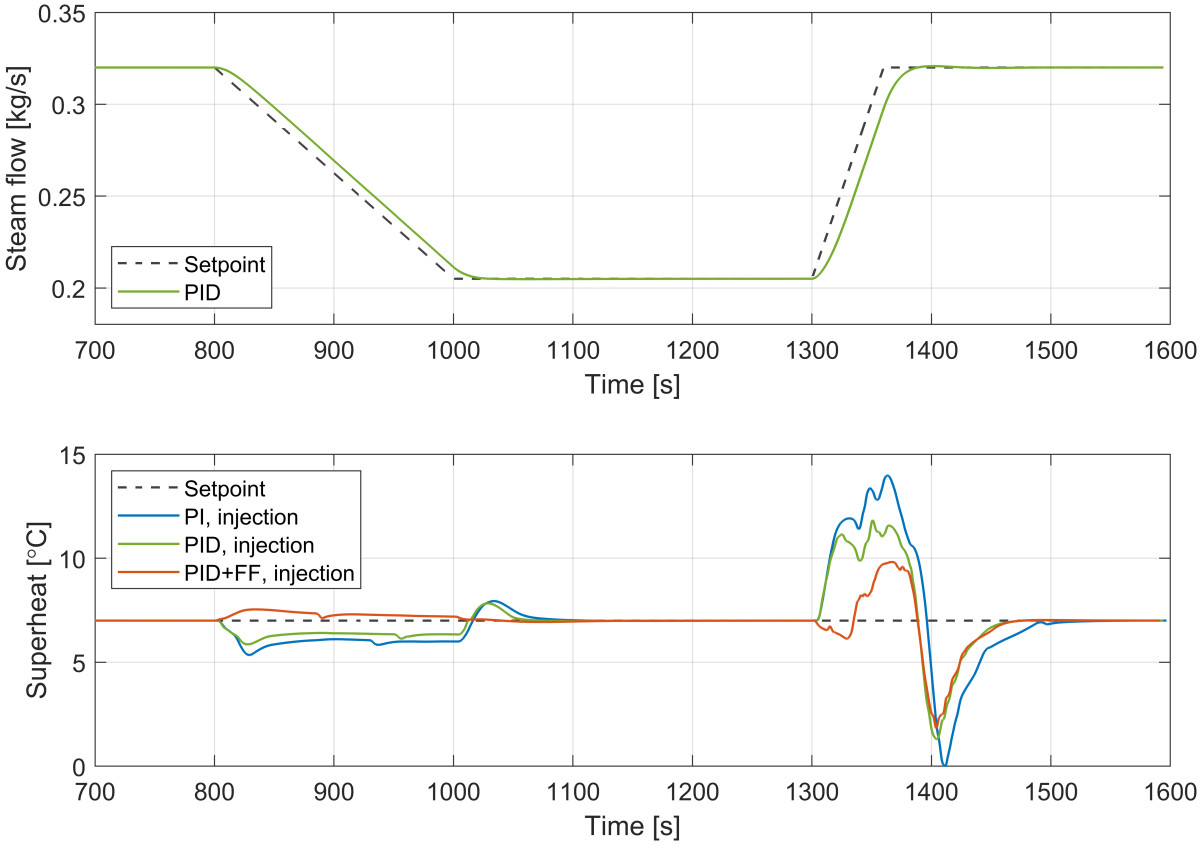

Figure 5.16: Comparison between PI, PID and PID plus feedforward control, at T_{water} = 80°C and p_{steam} = 2 bar(a)

From this figure it follows that there is indeed an immediate response. At 800 s, a significant increase in controller performance can be observed. The initial increase in superheat can be explained by the fact that the feedforward gain is not optimized for this specific operating condition, but is the mean of all. At the relatively fast ramp up at 1300 s, there is still a significant disturbance. Implementing cascade control, preferably with gain scheduling, is considered a good next step for further performance improvement.

5.2. Dynamic characteristics

In the previous section, the control system of the heat pump is optimized for flexible operation. In this section, the dynamic characteristics of the heat pump will be further analyzed and quantified. First the dynamic characteristics related to load level changes are discussed. In the second part, variations in waste heat water temperature and the associated risk is discussed.

5.2.1. Heat pump load variations

Currently, PI controllers are also used for heat pump control systems. As found in the previous section, these controllers are not an ideal choice for flexible operation. Despite improved performance of a PID based control system, the heat pump will still be limited in its ramping rate. This limitation is found to be caused by a disturbance in superheat during load level changes. Sufficient superheat should be guaranteed, to avoid damage to the compressor.

To analyze what the maximum ramp rate is, the compressor model is ramped up and down between 30 and 50 Hz in either 1, 2, 3 or 5 minutes. The system response is again analyzed at the same operating conditions as given in table 5.2. For a conservative approach, the controllers have only PID feedback capabilities, as optimized in subsection 5.1.2. The performance of the controllers, defined as the relation between the ramping rate and the maximum deviation in superheat, is presented in figure 5.17.

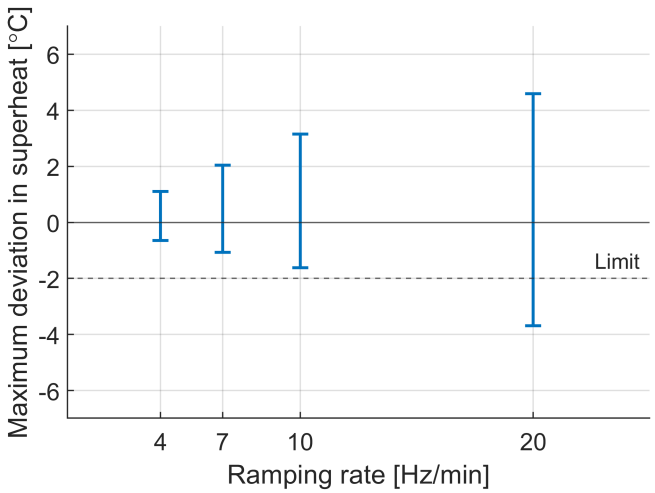

Figure 5.17: Maximum deviation in injection line superheat for different ramping rates

The maximum allowable decrease in superheat from the setpoint is determined to be 2°C. The margin between saturated conditions is thus 5°C. This margin is to account for the operating case where the waste heat water temperature increases simultaneously. The margin also allows for modeling errors. From figure 5.17, the maximum ramping rate follows and is found to be approximately 10 Hz/minute.

During load level changes, the superheat also shows a positive deviation from the setpoint. This affects the discharge temperature as well. As described in [11], a too high discharge temperature will cause oil degradation. From the analysis presented in [9], it becomes clear that this is however related to prolonged periods of operation. Furthermore, the absolute increase in discharge temperature is limited: at the maximum observed discharge temperature of 136.9°C, the additional increase was found to be only 2.5°C. The positive deviation in superheat is thus not considered a limiting factor for the maximum ramping rate.

In terms of reference tracking capabilities for steam demand response, a delay can be observed. The steam generation lags behind the steam demand by approximately 17 seconds. Note that this lag is relatively small in comparison to the maximum ramping rate of 10 Hz/minute.

5.2.2. Evaporator water temperature variations

Apart from variations in load level, the heat pump must ideally also be able to deal with variations in waste heat water temperature. Looking at the influence of such a variation on the superheat control system, figure 5.10, this effect can be considered small.

An important aspect, which is not directly related to the superheat control system, is the risk of condensation in the compressor suction lines. This risk was identified in a study focused on ammonia heat pumps for district heating by Meesenburg [44], and was related to load level changes. In the heat pump considered in this study, load level changes at constant waste heat water temperature and the previously determined maximum ramping rate only lead to a small change in suction gas temperature of ±2°C. This will thus not lead to condensation.

Rapid variations in waste heat water temperature could however lead to condensation. Whether condensation in the suction line does occur is not only dependent on the maximum deviation in superheat from the setpoint. This because in practice, the temperature of the suction tube wall lags behind the refrigerant bulk temperature. To study this effect in more detail, the waste heat water temperature is increased from 60°C to 80°C in 2 minutes. The refrigerant bulk temperature as well as the wall temperature of the suction tube are presented in figure 5.18 below.

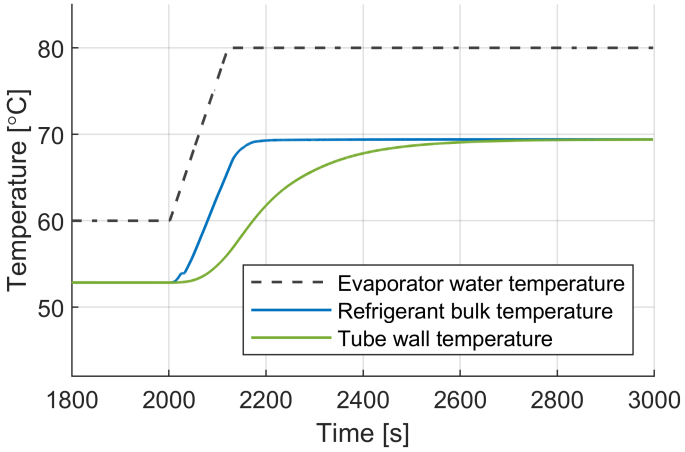

Figure 5.18: Temperature response of the refrigerant and tube wall at the compressor suction line during an increase in waste heat water temperature, at p_{steam} = 2 bar(a) and n = 50 Hz

From this figure the lag in the suction tube wall temperature follows. The maximum temperature difference between the refrigerant and the tube wall is found to be 10.3°C, which is larger than the 7°C of superheat. This gives the impression that condensation at the suction tube wall, in the viscous sublayer, will occur. The model is however not suitable to determine to what extent this is problematic. This because of the following reasons:

- First of all, the used heat transfer coefficient is a function of the bulk properties. In case condensation of refrigerant occurs in the viscous sublayer at the tube wall, the heat transfer model still assumes single phase cooling. In reality, this is not a valid assumption, as described in [33]. The deviation between conventional heat transfer modeling and reality is clearly depicted in figure 5.19. Also, the formation of condensate on the tube wall will result in an increased heat transfer rate to the tube wall, and thus to a reduced tube wall temperature lag. The behaviour presented in figure 5.18 can thus be considered conservative. In recent years, more attention is paid to the condensation of refrigerant from the superheated state. In a study by Agarwal and Hrnjak [6], and Xiao and Hrnjak [82], a model is presented that captures this phenomena as well. Application of these models is out of the scope of this study.
- Even with the integration of more advanced heat transfer models that do account for condensation from the superheated region, still no correct representation can be expected. This is caused by the way the suction tube model is discretized. The bulk region, as well as the tube wall, is only discretized in the axial direction. Therefore the radial temperature gradient is not representative.

From these considerations, it follows that further research is needed to quantify the effects of condensation. Note that in case the variation in waste heat water temperature is found to be too fast, the integration of mechanical solutions can be considered. Meesenburg [44] proposed the implementation of electrical heat tracing or the implementation of an internal heat exchanger. For implementation of the latter, see figure 2.2. Because both methods introduce an increase in CAPEX, the incentive to implement these solutions might be small. A solution that might sufficiently counteract condensation effects and is relatively simple, is the use of an internally ribbed or finned suction tube. This will increase the heat transfer coefficient, and thus reduce the tube wall temperature lag. To what extent this solution can aid in mitigating condensation requires further investigation and is out of the scope.

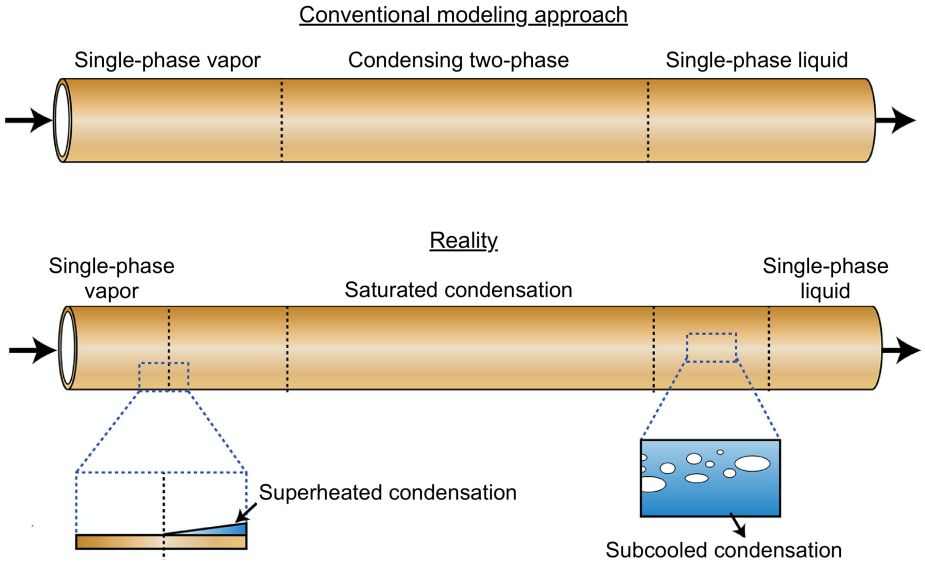

Figure 5.19: Comparison between the conventional heat transfer modeling approach and reality. Adapted from [33]

6

Conclusions and Recommendations

In this final chapter, first the conclusions that follow from the presented study are provided. In the second part, recommendations related to future research opportunities are discussed.

6.1. Conclusions

This study is aimed at making industrial sized heat pump systems a more attractive solution for industrial heating purposes, by studying the potential of flexible operation. The study demonstrates that flexibility of industrial, high temperature heat pumps can be improved to such an extent, that the equipment becomes suitable for heat demand response application. At these levels of flexibility, participation in grid load balancing pools or electricity market response is possible as well, which has financial benefits.

Quantitatively speaking, the high temperature industrial heat pump considered in this report is found to be able to ramp up and down at a maximum rate of 20%/min. The limiting factor in this economizer cycle is the ability of the control system to keep the superheat at the screw compressor injection port within acceptable limits. The steam demand response delay is found to be in the order of 17 s. Relative to the ramping rate, this can be considered small.

Note that the aforementioned conclusions are related to flexibility in load level changes. When looking at flexibility in the supply of heat to the heat pump, a risk is identified which can be extrapolated to other heat pump systems as well. During a relatively fast increase in waste heat water temperature, there is a risk of condensation in the suction line, as presented in subsection 5.2.2. This does not put a constraint on the maximum load level ramping rate of the heat pump. Solutions that could solve or mitigate this problem are implementation of an internal heat exchanger, the application of heat tracing on the suction tube, or possibly the application of an internally finned suction tube.

The obtained flexibility level can be achieved using the conventional SISO PID control structure. Moreover, the identified flexibility limits of the heat pump can be improved further by implementing additional control structures. Structures considered in this study are feedforward, cascade control and gain scheduling, in decreasing order of expected performance improvement. The fact that the presented level of flexibility can be achieved without these structures is beneficial, because it might promote the uptake in industry as no substantial increase in development costs is brought along.

The presented control system tuning approach can be considered generally applicable, either by using a dynamic model, or by using solely experimental data. This allows for extrapolation of the approach to other heat pump systems. The same applies to the modeling approach, which is found to be suitable for the dynamic characterization. Because the model is block diagram based, the component models can be used for the modeling of other heat pump cycle layouts.

6.2. Recommendations

Although the presented study provides closure on the main research objectives, new questions are unveiled as well. In this section, the most relevant questions that should be addressed in future studies are discussed.

It is first of all recommended to extent this study with experimental validation. The results in this study are based on calibration and validation using manufacturer data. Although this is accounted for by applying a conservative approach, experimental validation of the model is still recommended to increase the accuracy of the results. Furthermore, experimental validation will also give more insight. For example in the origination of losses in the screw compressor, or in the behavior of the heat pump during variations in steam pressure. This behavior could then be implemented in the model as well.

Another aspect that requires further investigation, is the formation of condensate during a rapid increase in waste heat water temperature. Condensate in the compressor suction line poses a risk for safe operation. Because the developed heat pump model is not sufficiently detailed for a quantitative condensate analysis, it is recommended to develop a more detailed model of the suction tube. With this model, advanced heat transfer models can be used to quantify the behavior. Another method that can be employed to obtain more insight into the condensation process is experimental analysis.

Out of the scope of this study, but considered valuable to promote the availability of flexible industrial heat pumps, is a thorough business case analysis. Apart from the theoretical, and in the future also practical demonstration of flexible operation, it is recommended to quantify the financial benefit of dynamic operation as well. It is recommended to develop the business case for different types of operation. A distinction can be made between batch and continuous processes. For the business case analysis, it is recommended to develop an operational strategy that takes advantage of the energy price fluctuations.

Of influence on the financial benefits of flexible operation is the cycle performance at off-conditions. It is recommended to investigate to what extent the use of a variable volume ratio compressor increases the cycle efficiency. In the current configuration, energy losses due to under- and overcompression negatively affect the performance at off-conditions.

Bibliography

[1] Low capex industrial heat pump (in paper industry). URL https://projecten.topsectorenergie.nl/projecten/low-capex-industrial-heat-pump-in-paper.-industry-00029079.

[2] *VDI Heat Atlas*. Springer-Verlag Berlin Heidelberg, 2 edition, 2010. doi: 10.1007/978-3-540-77877-6.

[3] Netcode elektriciteit, kenmerk BWBR0037940, 2020. URL https://wetten.overheid.nl/BWBR0037940.

[4] Productinformatie automatic Frequency Restoration Reserve. Technical report, Tennet, 2020. URL https://www.tennet.eu/fileadmin/user_upload/SO_NL/Productinformatie_aFRR.pdf.

[5] S. Abdan, N. Stosic, A. Kovacevic, I. Smith, and P. Deore. Identification and analysis of screw compressor mechanical losses. *IOP Conference Series: Materials Science and Engineering*, 425 (1), 2018. ISSN 1757899X. doi: 10.1088/1757-899X/425/1/012015.

[6] R. Agarwal and P. Hrnjak. Effect of sensible heat, condensation in superheated and subcooled region incorporated in unified model for heat rejection in condensers in horizontal round smooth tubes. *Applied Thermal Engineering*, 71(1):378–388, 2014. ISSN 1359-4311. doi: https://doi.org/10.1016/j.applthermaleng.2014.05.071. URL https://www.sciencedirect.com/science/article/pii/S1359431114004475.

[7] AGC Inc. AMOLEA 1224yd. 1:1–6, 2019.

[8] C. Arpagaus. *Hochtemperatur-Wärmepumpen: Marktübersicht, Stand der Technik und Anwendungspotenziale*. VDE Verlag GmbH, 2018. ISBN 9783800745517.

[9] C. Arpagaus and S. Bertsch. Experimental results of hfo/hcfo refrigerants in a laboratory scale hthp with up to 150 °c supply temperature. 09 2019.

[10] C. Arpagaus, F. Bless, Jürg S., and S.S. Bertsch. Pompes à chaleur à multiples températures: Une synthèse de la littérature. *International Journal of Refrigeration*, 69:437–465, 2016. ISSN 01407007. doi: 10.1016/j.ijrefrig.2016.05.014. URL http://dx.doi.org/10.1016/j.ijrefrig.2016.05.014.

[11] C. Arpagaus, F. Bless, M. Uhlmann, J. Schiffmann, and S.S. Bertsch. High temperature heat pumps: Market overview, state of the art, research status, refrigerants, and application potentials. *Energy*, 152:985–1010, 6 2018. ISSN 03605442. doi: 10.1016/j.energy.2018.03.166. URL https://doi.org/10.1016/j.energy.2018.03.166.

[12] C. Arpagaus et al. High temperature heat pump using hfo and hcfo refrigerants - system design, simulation, and first experimental results. 08 2018. doi: 10.18462/iir.icr.2019.242.

[13] K.J. Astrom and R.M. Murray. *Feedback Systems: An Introduction for Scientists and Engineers*. Princeton University Press, USA, 2008. ISBN 0691135762.

[14] E.B. Broerman, T. Manthey, J. Wennemar, and J. Hollingsworth. *Screw compressors*. 2018. ISBN 9780128146835. doi: 10.1016/B978-0-12-814683-5.00006-7.

[15] P. Byrne, R. Ghoubali, and J. Miriel. Scroll compressor modelling for heat pumps using hydrocarbons as refrigerants. *International Journal of Refrigeration*, 41:1–13, 2014. ISSN 01407007. doi: 10.1016/j.ijrefrig.2013.06.003. URL http://dx.doi.org/10.1016/j.ijrefrig.2013.06.003.

[16] Y.A. Cengel. *Heat and Mass Transfer: A Practical Approach*. McGraw-Hill, 3 edition, 2006. ISBN 9780071257398.

[17] M. Chamoun, R. Rulliere, P. Haberschill, and J.F. Berail. Dynamic model of an industrial heat pump using water as refrigerant. *International Journal of Refrigeration*, 35(4):1080–1091, 2012. ISSN 01407007. doi: 10.1016/j.ijrefrig.2011.12.007.

[18] J.G. Collier and J.R. Thome. *Convective Boiling and Condensation*. Oxford engineering science series. Clarendon Press, 3 edition, 1996. ISBN 9780198562962.

[19] L. Dardenne, E. Fraccari, A. Maggioni, L. Molinaroli, L. Proserpio, and E. Winandy. Semi-empirical modelling of a variable speed scroll compressor with vapour injection. *International Journal of Refrigeration*, 54:76–87, 2015. ISSN 01407007. doi: 10.1016/j.ijrefrig.2015.03.004. URL http://dx.doi.org/10.1016/j.ijrefrig.2015.03.004.

[20] R. De Boer et al. Strengthening Industrial Heat Pump Innovation, Decarbonizing Industrial Heat, White Paper. pages 1–32, 2020.

[21] S. Egner. Subcooling and Superheat: Superheroes of System Charging | Contracting Business, 8 2016. URL https://www.contractingbusiness.com/service/article/20868656/subcooling-and-superheat-superheroes-of-system-charging.

[22] A. El Gammal. Achieving paris agreement: One covid-19 crisis per year until 2050. URL http://www.europeanenergyinnovation.eu/Articles/Summer-2020/Achieving-Paris-Agreement-One-Covid-19-crisis-per-year-until-2050.

[23] Modelica Association et al. Modelica Standard Library. URL https://modelica.org/libraries/ModelicaLibrariesOverview.html.

[24] A. Faghri and Y. Zhang. *Fundamentals of Multiphase Heat Transfer and Flow*. Springer International Publishing, 2020. doi: 10.1007/978-3-030-22137-9.

[25] W.P.D. Fernando. *Experimental Investigation of Refrigerant Charge Minimisation of a Small Capacity Heat Pump*. PhD thesis, Royal Institute of Technology, 2007.

[26] *RC2-G/T Technical manual*. Hanbell Precise Machinery Co. Ltd., 12 2020.

[27] Honeywell International Inc. Honeywell Solstice ® Refrigerants Solstice ® refrigerants roadmap : The future of refrigerants. (1):1–2, 2016.

[28] G.F. Hundy, A.R. Trots, and T.C. Welch. Chapter 4 - Compressors. In *Refrigeration, Air Conditioning and Heat Pumps*, pages 59–87. Butterworth-Heinemann, 5 edition, 2016. ISBN 9780081006665.

[29] IEA. Renewables 2019. Technical report, IEA, Paris, 2019. URL https://www.iea.org/reports/renewables-2019/heat.

[30] The MathWorks Inc. Control System Toolbox™, . URL https://nl.mathworks.com/products/control.html.

[31] The MathWorks Inc. PID Tuning Algorithm, . URL https://nl.mathworks.com/help/control/getstart/pid-tuning-algorithm.html.

[32] IRC. Variable Frequency Drive Opportunities in Industrial Refrigeration Systems. *The Cold Front*, 4(2):1–9, 2004.

[33] T.A. Jacob and B.M. Fronk. A heat transfer model to predict superheated and saturated condensation of hfc/hfo refrigerant mixtures. *International Journal of Heat and Mass Transfer*, 170:120947, 2021. ISSN 0017-9310. doi: https://doi.org/10.1016/j.ijheatmasstransfer.2021.120947. URL https://www.sciencedirect.com/science/article/pii/S0017931021000508.

[34] T. Kaida, I. Sakuraba, K. Hashimoto, and H. Hasegawa. Experimental performance evaluation of heat pump-based steam supply system. In *IOP Conference Series: Materials Science and Engineering*, volume 90. Institute of Physics Publishing, 7 2015. doi: 10.1088/1757-899X/90/1/012076.

[35] S.A. Klein and F.L. Alvarado. Engineering equation solver. *F-Chart Software, Madison, WI*, 1, 2002.

[36] G. Kosmadakis. Estimating the potential of industrial (high-temperature) heat pumps for exploiting waste heat in EU industries. *Applied Thermal Engineering*, 156(December 2018):287–298, 2019. ISSN 13594311. doi: 10.1016/j.applthermaleng.2019.04.082. URL https://doi.org/10.1016/j.applthermaleng.2019.04.082.

[37] R. Kumar, S. Singla, and V. Chopra. Comparison among some well known control schemes with different tuning methods. *Journal of Applied Research and Technology*, 13:409–415, 06 2015. doi: 10.1016/j.jart.2015.07.007.

[38] C. Le Quéré et al. Temporary reduction in daily global CO2 emissions during the COVID-19 forced confinement. *Nature Climate Change*, 10(7):647–653, 2020. ISSN 17586798. doi: 10.1038/s41558-020-0797-x. URL http://dx.doi.org/10.1038/s41558-020-0797-x.

[39] E.W. Lemmon, I.H. Bell, M.L. Huber, and M.O. McLinden. NIST Standard Reference Database 23: Reference Fluid Thermodynamic and Transport Properties-REFPROP, Version 10.0, National Institute of Standards and Technology, 2018. URL https://www.nist.gov/srd/refprop.

[40] B. Li and A.G. Alleyne. A dynamic model of a vapor compression cycle with shut-down and start-up operations. *International Journal of Refrigeration*, 33(3):538–552, 2010. ISSN 01407007. doi: 10.1016/j.ijrefrig.2009.09.011. URL http://dx.doi.org/10.1016/j.ijrefrig.2009.09.011.

[41] G.D. Librado, E.E. Rodríguez Vázquez, L. Alvaro, M. Santiyanes, J. Hernán Pérez Vázquez, C. Alexander, and N. Martín. Transient Analysis of a Single-stage Vapor Compression Refrigeration System Using Lumped Parameter Approaches Analysis and simulation validation based on a reduced order differential equation with few degrees of freedom. *International Journal on Advances in Systems and Measurements*, 11(3):352–362, 2018. URL http://www.iariajournals.org/systems_and_measurements/2018,.

[42] J. Ma, D. Kim, and J. Braun. Development of a fast method for retrieving thermodynamic properties to accelerate transient vapor compression cycle simulation. 2018.

[43] A. Marina, S. Spoelstra, H.A. Zondag, and A.K. Wemmers. An estimation of the European industrial heat pump market potential. *Renewable and Sustainable Energy Reviews*, pages 1–15, 2021. doi: https://doi.org/10.1016/j.rser.2020.110545.

[44] W. Meesenburg. *Heat pumps supplying district heating and ancillary services for the power system*. PhD thesis, Technical University of Denmark, 2020.

[45] W. Meesenburg, W. Brix Markussen, T. Ommen, and B. Elmegaard. Optimizing control of two-stage ammonia heat pump for fast regulation of power uptake. *Applied Energy*, 271(May):115126, 2020. ISSN 03062619. doi: 10.1016/j.apenergy.2020.115126. URL https://doi.org/10.1016/j.apenergy.2020.115126.

[46] R.W. Miller. *Flow Measurement Engineering Handbook*. McGraw-Hill, 1989. ISBN 9780070420465.

[47] A.F. Mills and C.F.M. Coimbra. *Basic Heat and Mass Transfer*. Temporal Publishing, LLC, 3 edition, 2015. ISBN 9780996305303.

[48] Modelica Association. Modelica® - A Unified Object-Oriented Language for Physical Systems Modeling. {Tutorial}, 12 2000. URL http://www.modelica.org/documents/ModelicaTutorial14.pdf.

[49] H. Moisi and R. Rieberer. Refrigerant Selection and Cycle Development for a High Temperature Vapor Compression Heat Pump. *12th IEA Heat Pump Conference 2017, Rotterdam*, pages 1–10, 2017.

[50] R.A. Mollenkamp. *Control of High-Order Systems Using Simple Models.* PhD thesis, LSU Historical Dissertations and Theses, 1971. URL https://digitalcommons.lsu.edu/gradschool_disstheses/1938.

[51] C.U. Moon et al. Experimental study on the performance of the vapor injection refrigeration system with an economizer for intermediate pressures. *Heat and Mass Transfer/Waerme- und Stoffuebertragung*, 54(10):3059–3069, 2018. ISSN 14321181. doi: 10.1007/s00231-018-2359-6.

[52] M.J. Moran, H.N. Shapiro, D.D. Boettner, and M.B. Bailey. *Principles of Engineering Thermodynamics*. Wiley, 2015. ISBN 9781118960882.

[53] Nederlandse Organisatie voor toegepast natuurwetenschappelijk onderzoek TNO. Full Scale Industrial Heat Pump Using Natural Refrigants, 2019. URL https://projecten.topsectorenergie.nl/projecten/full-scale-industrial-heat-pump-using-natural-refrigants-00031620.

[54] P. Nellissen and S. Wolf. Heat pumps in non-domestic applications in Europe - Potential for an energy revolution, 2015.

[55] OSMC. OpenModelica User's Guide. 2021. URL https://openmodelica.org/doc/OpenModelicaUsersGuide/OpenModelicaUsersGuide-latest.pdf.

[56] P.A. Pérez, P. Albertos, A. Sala, and S. Antonio. *Multivariable Control Systems: An Engineering Approach*. Advanced Textbooks in Control and Signal Processing. Springer, 2004. ISBN 9781852337384.

[57] L. Petzold. Differential/algebraic equations are not ode's. *Siam Journal on Scientific and Statistical Computing*, 3, 09 1982. doi: 10.1137/0903023.

[58] L.R. Petzold. Description of DASSL: A differential/algebraic system solver. page 9, Livermore, 1982. Sandia National Laboratories.

[59] H. Qiao, V. Aute, and R. Radermacher. Transient modeling of a flash tank vapor injection heat pump system - Part I: Model development. *International Journal of Refrigeration*, 49:169–182, 2015. ISSN 01407007. doi: 10.1016/j.ijrefrig.2014.06.019. URL http://dx.doi.org/10.1016/j.ijrefrig.2014.06.019.

[60] H. Qiao, X. Xu, V. Aute, and R. Radermacher. Transient modeling of a flash tank vapor injection heat pump system - Part II: Simulation results and experimental validation. *International Journal of Refrigeration*, 49(1):183–194, 2015. ISSN 01407007. doi: 10.1016/j.ijrefrig.2014.06.018. URL http://dx.doi.org/10.1016/j.ijrefrig.2014.06.018.

[61] B.P. Rasmussen. Dynamic modeling for vapor compression systems-Part I: Literature review, 2012. ISSN 10789669.

[62] C.C. Richter. Proposal of New Object-Oriented Equation-Based Model Libraries for Thermodynamic Systems. PhD Thesis. *PhD Thesis*, 2008.

[63] D. Shah and D.M. Joshi. Comparative Study of Slide Valve and Variable Frequency Drive for Screw Compressor Control System Comparative Study of Slide Valve and Variable Frequency Drive for Screw Compressor Control System Medical Science. *Indian Journal of Applied Research*, 5(1):8–11, 2015. URL https://www.worldwidejournals.com/indian-journal-of-applied-research-(IJAR)/special_issues_pdf/January_2015_1422603381__84.pdf.

[64] M.M. Shah. A general correlation for heat transfer during film condensation inside pipes. *International Journal of Heat and Mass Transfer*, 22(4), 1979. ISSN 00179310. doi: 10.1016/0017-9310(79)90058-9.

[65] *Modulating control valves with magnetic actuators, PN 16*. Siemens Switzerland Ltd., 2 2018.

[66] TLK-Thermo GmbH. TIL 3.9.1, TILMedia 3.9.1, ModelFitter, 2020. URL https://www.tlk-thermo.com/index.php/en/.

[67] TNO. Heat pump test rig, 2020.

[68] E. Trømborg, M. Havskjold, T.F. Bolkesjø, J.G. Kirkerud, and A.G. Tveten. Flexible use of electricity in heat-only district heating plants. *International Journal of Sustainable Energy Planning and Management*, 12:29–46, 2017. ISSN 22462929. doi: 10.5278/ijsepm.2017.12.4.

[69] W. Tuchowski and K. Kurtz-Orecka. The Impact of Refrigerants on the Efficiency of Automotive Air-Conditioning System. In P. Ball, L. Huaccho Huatuco, R.J. Howlett, and R. Setchi, editors, *Sustainable Design and Manufacturing 2019*, pages 615–623, Singapore, 2019. Springer Singapore. ISBN 978-981-13-9271-9.

[70] T.M. Tveit. Application of an industrial heat pump for steam generation using district heating as a heat source. In *12th IEA Heat Pump Conference 2017, Rotterdam*, number 1395, 2017.

[71] United Nations Environment Programme. *Emissions Gap Report 2019*. Nairobi, 2019. ISBN 9789280737660.

[72] United States. Federal Emergency Management Agency and United States. Department of Transportation and United States. Environmental Protection Agency. *Handbook of Chemical Hazard Analysis Procedures*. Federal Emergency Management Agency, Washington, 1989.

[73] L.L. Van Bommel. Thermodynamic Model of a Screw Compressor. (August), 2016. URL http://repository.tudelft.nl/.

[74] P. van den Berg, C. Feijen, and R. de Vette. De elektriciteitsmarkt in vogelvlucht. Technical report, Agro Energy, 2017. URL https://www.agro-energy.nl/wp-content/uploads/2017/03/Whitepaper_Energiemarkt_in_vogelvlucht_LR.pdf.

[75] G.M. van der Zalm. *Tuning of PID-type controllers: literature overview*. DCT rapporten. Technische Universiteit Eindhoven, 2004. DCT 2004.054.

[76] T.T.S. Wan. Engineered Industrial Refrigeration Systems Application. pages 60–85, 2008.

[77] D. Wang, B. Yu, J. Shi, and J. Chen. Experimental and theoretical study on the cooling performance of a co2 mobile air conditioning system. *Energies*, 11(8), 2018. ISSN 1996-1073. doi: 10.3390/en11081927. URL https://www.mdpi.com/1996-1073/11/8/1927.

[78] M. Willatzen, N. Pettit, and L. Ploug-S\o{}rensen. A general dynamic simulation model for evaporators and condensers in refrigeration. Part I: moving-boundary formulation of two-phase flows with heat exchange. *International Journal of Refrigeration*, 21(5):398–403, 1998. URL http://www.sciencedirect.com/science/article/pii/S0140700797000911.

[79] E.L. Winandy and J. Lebrun. Scroll compressors using gas and liquid injection: Experimental analysis and modelling. *International Journal of Refrigeration*, 25(8):1143–1156, 2002. ISSN 01407007. doi: 10.1016/S0140-7007(02)00003-8.

[80] P.J. Woolf. *Chemical Process Dynamics and Controls*. Open textbook library. University of Michigan Engineering Controls Group, 2009.

[81] H. Wu, J. Li, and Z. Xing. Theoretical and experimental research on the working process of screw refrigeration compressor under superfeed condition, 2007. ISSN 01407007.

[82] J. Xiao and P. Hrnjak. A heat transfer model for condensation accounting for non-equilibrium effects. *International Journal of Heat and Mass Transfer*, 111:201–210, 2017. ISSN 0017-9310. doi: https://doi.org/10.1016/j.ijheatmasstransfer.2017.03.019. URL https://www.sciencedirect.com/science/article/pii/S0017931016337280.